Developmental Plasticity and Stromal Co-option Shape a Pituitary Neuroendocrine Tumor Transcriptional Continuum

Robert C. Osorio[1]*, Jun Y. Oh[1]*, Ankita Sati[1]*, Jangham Jung[1]*, Alexander J. Ehrenberg[2,3], Atul Saha[1], Meeki Lad[1], Harmon Khela[1], Nicole Brennick[2], Petros Giannikopoulos[2,4], William W. Seeley[3], Lea T. Grinberg[3], Aaron Diaz[1], Manish K. Aghi[1]

***Contributed equally**

[1]Department of Neurological Surgery, University of California San Francisco, San Francisco, CA

[2]Innovative Genomics Institute, Berkeley, CA

[3]Department of Neurology, Weill Institute of Neuroscience, Memory and Aging Center, University of California San Francisco, San Francisco, CA

[4]Department of Laboratory Medicine, University of California, San Francisco, CA

Running Title: Developmental Plasticity and Stromal Interactions in Pituitary Tumor Transcriptional Dynamics

Keywords: pituitary adenoma, pituitary tumor, PitNET, tumor microenvironment, single-nuclei RNA sequencing, spatial transcriptomics, prolactinoma, Cushing's

Abstract

Pituitary neuroendocrine tumors (PitNETs) are common intracranial neoplasms with complex biology underpinned by unresolved cellular origins, molecular heterogeneity, and microenvironment interactions. Here, we employ single-nuclei RNA-sequencing (snRNA-seq) of 419,874 cells from human normal pituitaries and PitNETs with spatial transcriptomics to resolve these challenges. We identify multi-hormonal neuroendocrine cells in both normal and tumor tissues, originating as early pseudotime intermediates from pituitary stem cells, revealing an inherent plasticity that blurs traditional lineage boundaries. PitNETs exhibit a transcriptional continuum across subtypes, challenging their classification into discrete categories. Trajectory analysis uncovers divergent cellular origins: silent gonadotroph adenomas (SGAs), prolactinomas, silent corticotroph adenomas (SCAs), and Cushing's adenomas are closely linked to differentiated neuroendocrine cells, while somatotroph and null cell adenomas (NCAs) appear to derive more directly from adult stem cells. Tumor cells co-opt robust cell-cell communication networks found in normal adult neuroendocrine cells. Spatial profiling further demonstrates that perivascular niches enhance tumorigenicity through angiogenic and epithelial-mesenchymal transition programs. Our work redefines PitNETs as ecosystems shaped by developmental plasticity and microenvironmental crosstalk, offering a roadmap for future therapies targeting lineage fluidity and stromal dependencies.

1. Introduction

Pituitary neuroendocrine tumors (PitNETs, previously known as pituitary adenomas) are common intracranial tumors originating from the anterior pituitary gland. Nearly half of PitNETs overproduce hormones and cause symptoms specific to their neuroendocrine type. For instance, hypersecreting lactotroph tumors (prolactinomas) lead to galactorrhea. Hypersecreting somatotroph tumors cause acromegaly, while hypersecreting corticotroph tumors lead to Cushing's disease. In contrast, some PitNETs remain hormonally silent and primarily manifest as mass effects or are incidentally diagnosed. While most silent PitNETs are silent gonadotrophs, all types of hypersecreting PitNETs can have a silent counterpart.

The 2017 World Health Organization (WHO) classification brought a paradigm shift by categorizing pituitary tumors based on cell lineage, determined through the immunohistochemical expression of three transcription factors (TFs) implicated in the development of the various subtypes of normal neuroendocrine cells, with TPIT (TBX19) immunopositivity identifying corticotrophic PitNETs; PIT1 immunopositivity identifying somatotroph, lactotroph, or thyrotroph PitNETs; SF1 immunopositivity identifying gonadotroph PitNETs, and triple-negative immunostaining identifying null cell PitNETs. This new approach deviates from the previous reliance solely on hormone type and is maintained in the 2022 WHO classification[1,2]. While the pituitary cell lineage classification system represents a notable insight, the complex process of PitNET tumorigenesis and the dynamics of TF expression are not yet fully understood. Additionally, it remains uncertain whether the presence of PitNETs with multiple transcriptional signatures or varying degrees of differentiation[3,4] necessitates the need for a more flexible subtyping approach, as their nature may be more fluid than previously presumed.

Previous molecular studies of PitNETs have been constrained by methodological limitations. Bulk RNA sequencing obscures cellular diversity[4], while prior single-cell analyses[3,5–7] hindered by small cohorts, cell dissociation artifacts, and sparse spatial resolution—fail to resolve rare subpopulations or microenvironmental interactions. Here, we leverage snRNA-seq to profile 419,874 nuclei from 11 PitNETs and two normal pituitary glands, bypassing dissociation bias in fragile neuroendocrine cells[8,9], and integrate spatial transcriptomics. We map the developmental trajectories of PitNET subtypes, decode their stromal

105 crosstalk, and reconstruct a high-resolution atlas of human pituitary glands and PitNETs. Our findings
106 redefine PitNETs as ecosystems shaped by lineage fluidity and microenvironmental hijacking, offering a
107 roadmap to refine diagnostic and therapeutic frameworks.
108

109 **2. Results**

110 **2.1 Single-nuclei atlas of adult human pituitary glands**

111 To elucidate the cellular composition and transcriptional dynamics of the normal adult human
112 pituitary gland, we performed single nuclear RNA-sequencing (snRNA-seq) on postmortem pituitary
113 glands collected from non-tumor subjects (n=2) with short postmortem intervals (PMI < 10 hours) **(Fig.**
114 **1a).** After implementing rigorous quality control and filtering steps, we obtained 29,071 high-quality nuclei,
115 with an average of 6,540 unique molecular identifiers (UMIs) and 2,643 genes per nucleus. To reduce the
116 dimensionality and identify nuclei with similar transcriptomic patterns, we implemented Principles
117 Component Analysis (PCA) and Uniform Manifold Approximation and Projection (UMAP) algorithm
118 using Seurat software[10], resulting in 17 distinct nuclei clusters present in both samples **(Fig. 1b-d)**. Using
119 canonical gene markers from previous studies[3,11] and SingleR[12], we identified all five types of
120 neuroendocrine cells (corticotroph, gonadotroph, lactotroph, thyrotroph, somatotroph), immune cells
121 (macrophage, T cells), stromal cells (pituicyte, pericyte, endothelial cells), and adult pituitary stem cells
122 **(Fig. 1b, e)**. Each cluster contained cells from both donors, and the percentage of cells from each sex was
123 similar, suggesting minimal batch effect **(Fig. 1c, d)**.

124 Consistent with previous findings on pluripotent stem cells in the anterior pituitary[13–16], our stem
125 cell cluster exhibited high expression of genes *RBPMS*, *LGR4*, and *GRHL2* **(Fig. 1e)**. The stem cell cluster
126 also expressed a greater number of TF genes than mature neuroendocrine cells, including TF genes
127 previously described in human fetal pituitary (i.e., *PROP1*, *NFIB*, *LHX3*, *HEY1*, *ZNF521*)[11] and 48 novel
128 pituitary TF genes **(Supplementary Table 1).** Gene ontology analysis of the upregulated genes in the stem
129 cells revealed enrichment in processes related to epithelium development and cell morphogenesis,
130 consistent with their stem-like identity.

131 An interesting finding emerging from our single nuclei atlas of the adult human pituitary gland was
132 four clusters (20% of total cells in normal control samples) exhibiting co-expression of various
133 neuroendocrine transcriptomic signatures. These clusters were designated pluri-hormonal clusters 1-4 as
134 follows: (1) pan-hormonal (somatotroph/lactotroph/corticotroph/gonadotroph), (2)
135 somatotroph/gonadotroph, (3) somatotroph/lactotroph, also known as somatomammotroph,[17] and (4)
136 lactotroph/thyrotroph **(Fig. 1b, e)**. Previous studies using immunohistochemistry have observed PIT-1
137 lineage plurihormonal tumor cells[2,18,19], rarer multi-lineage plurihormonal tumor cells[20], and the presence
138 of plurihormonal cells in the normal adult human anterior pituitary.[21] However, the classification of
139 plurihormonal cells as distinct cell lineage or as intermediate stages between different lineages remains a
140 subject of debate.[22–24] To investigate further, we conducted pseudotime trajectory analysis[25,26] to explore
141 the developmental progression of plurihormonal cells relative to stem cells and classical monohormonal
142 neuroendocrine cells **(Fig. 1f, g)**. We found that monohormonal gonadotroph and corticotroph cells
143 diverged from stem cells early in our pseudotime, suggesting early differentiation of TPIT and SF-1 lineage,
144 respectively, with few intermediate states. This finding differs with a previous snRNA-seq study involving
145 4113 cells, which reported more intermediate states for both gonadotroph and corticotroph cells.[11] In
146 contrast to TPIT and SF-1 lineage, PIT1-lineage cells (i.e., lactotroph, somatotroph, and thyrotroph cells)
147 emerged in the middle or late stages of pseudotime **(Fig. 1g).** Interestingly, pan-hormonal cluster appeared
148 early in pseudotime, whereas plurihormonal clusters 2, 3, and 4 emerged later **(Fig. 1g)**, suggesting that,
149 while the latter plurihormonal clusters represent terminal states with possible secreting functional capability,
150 pan-hormonal cluster, which co-expresses transcription markers for four endocrine type cells, might
151 represent a transient, intermediate state that undergoes additional pruning or specialization in response to
152 physiological demands or pathological stimuli. [27–29]

153 Next, we leveraged pseudotime analysis to identify key TFs associated with the development of
154 each endocrine cell type from stem cells **(Supplementary Figs. 1-8; Supplementary Table 2)**. Certain TF
155 genes, such as *ST18* and *ZBTB16*, exhibited increased expression across multiple cell lineages, suggesting
156 their broader role in general neuroendocrine differentiation Notably, *MYT1L* and *ZNF10* displayed

157 increased expression in all three PIT-lineage neuroendocrine cells, while *NR4A1* exhibited specific
158 upregulation in thyrotroph and lactotroph cells. Estrogen Receptor 1 (*ESR1*), a ligand-activated TF, was
159 associated with both gonadotroph and lactotroph maturation, in line with immunohistochemistry studies
160 demonstrating high expression of estrogen receptors in PRL, FSH, or LH-positive endocrine cells[30].
161 Additionally, nuclear receptor 4A2 (*NR4A2*), a member of the steroid-thyroid hormone-retinoid receptor
162 superfamily which directly binds the *PRL* promoter[31] showed increased expression during lactotroph
163 development **(Supplementary Fig. 4).** *NR4A2* is implicated in the establishment of dopaminergic systems
164 in the brain without a canonical ligand-binding domain, featuring instead a narrow and tight cavity for small
165 molecular ligands such as prostaglandins to bind[32,33].

166 Furthermore, cells in the four plurihormonal clusters we had identified expressed TF genes that
167 generally mirrored their hormonal-combination phenotype. For instance, in plurihormonal cluster 3
168 (somatotroph/lactotroph), we observed upregulation of somatotrophic differentiation-associated TF genes
169 (i.e., *HIF3A*, *PLAGL1*, *ZBTB16*) and lactotrophic differentiation-associated TF genes (i.e., *ESR1*, *NR4A1*,
170 *NR4A2*) over pseudotime, suggesting additive effects of TF activities in these plurihormonal cells. Finally,
171 we found that many stem cell-associated TF genes, including previously described genes (i.e., *GRHL2*,
172 *HMGA2*, *MECOM*, *NFIB*, *TCF7L1*, *ZNF521*[11]) and other novel genes (i.e., *RFX4*, *BNC2*, *EBF1*, *NFIB*,
173 *SETBP1*, *NPAS3*, *NFIA*) were downregulated during development across multiple cell lineages
174 (**Supplementary Fig. 1-8)**.
175

176 **2.2 Single-nuclei characterization of PitNET subtypes**

177 We then collected samples from 11 PitNETs (acromegaly (n=2), Cushing's adenoma (n=2), silent
178 corticotroph adenomas (SCA) (n=2), prolactinoma (n=2), silent gonadotroph adenomas (SGA) (n=2), and
179 null cell adenoma (NCA) (n=1)) during transsphenoidal surgeries for snRNA-seq. All tumor samples
180 underwent immunohistopathological examination of canonical PitNET markers using standard criteria[2]
181 **(Fig. 1a)**. After quality control, we obtained 390,718 nuclei from tumor samples, with an average of 327

182 UMIs and 116 genes per nucleus. We then reconstructed UMAP with 390,718 nuclei from tumor samples
183 and 29,071 nuclei from control samples **(Fig. 2a, b)**, yielding 29 distinct clusters.

184 At the snRNA transcriptomic level, integration of PitNET samples revealed distinct tumor clusters
185 with significant overlap, indicating a continuum within the subtypes rather than strict classification (**Fig.**
186 **2a, b)**. Hierarchical clustering based on the entire transcriptome further showed that silent corticotrophic
187 PitNETs clustered closely with silent gonadotroph PitNETs, while being distant from secreting
188 corticotrophic PitNETs **(Fig. 2c)**, suggesting a greater shared transcriptome across silent PitNETs than
189 across PitNETs with a shared hormonal staining but variable secretion patterns. Furthermore, despite
190 belonging to the PIT1 lineage family, prolactinomas and acromegaly adenomas did not cluster together
191 **(Fig. 2c).** These findings supported previous speculation[4,34] that lineage-specific TPIT, SF1, and PIT1
192 classification alone may not accurately reflect the cellular identities of these tumors.

193 We next examined large-scale chromosomal instability in pituitary tumors using single-cell large-
194 scale copy-number variations (CNVs) inferred by snRNA-seq **(Fig. 2d)**. Previous studies suggest that,
195 despite their predominantly benign nature, PitNETs often display arm-level copy-number alterations across
196 substantial portions of the genome[35], and these disruptions are present in the majority of individual tumor
197 cells[5]. Compared to control cells from the normal pituitary gland, we observed the most increased CNVs
198 across the genome in prolactinomas, while immune-negative null-cell adenoma showed the least alterations
199 in CNV **(Fig. 2d, e),** providing single-cell corroboration of previously reported microarray findings[36].
200 Unsupervised hierarchical clustering of PitNETs based on CNV profiles revealed two key findings. First,
201 CNV changes are specific to tumor subtypes, with somatotrophic and null cell PitNETs showing the least
202 CNV changes and lactotrophic PitNETs showing the most CNV changes (**Fig. 2f**). Second, silent
203 corticotrophic PitNETs are a distinct subtype with a unique CNV profile far more altered than secreting
204 corticotrophic PitNETs rather than a subtle modification of secreting corticotrophic PitNETs **(Fig. 2f).**

205 Our snRNA-seq transcriptome-wide analysis corroborated previously described gene expression
206 biomarkers[3,37] for somatotrophic (e.g. *GH1*, *GHRHR*, *ENPP1*), secreting corticotrophic (e.g. *POMC*), silent
207 corticotrophic (e.g. *TBX19*), lactotrophic (e.g. *PRL*, *ENO3*, *NTS*), and silent gonadotrophic (i.e., FSHB,

208 CHGA, TGFBR3L) PitNETs. Null-cell adenomas were negative for these specific genes. We discovered
209 novel TFs that are tumor subtype-specific, including somatotrophic (*HOB4*, *NKX2-2*, *HOB3*, *NPAS4*,
210 *PRDM8*), secreting corticotrophic (*TFCP2L1*, *BNC2*, *CUX2*, *ARNTL2*, *LIN28B*), lactotrophic (*VDR*,
211 *ZNF831*, *ZNF521*, *RARB*, *CXXC5*), silent gonadotrophic (*TCF7*, *L3MBTL3*, *ZNF213*, *SCRT1*, *PROX1*),
212 and NCA (*ONECUT1*, *ZNF804A*, *MKX*, *PRRX1*, *L3MBTL4*) **(Supplementary Table 3)**. Notably, we also
213 identified increased expression of TF genes, such as *PPARG*, *NR2F2*, and *SOX5*, in PitNETs that can be
214 targeted using ligand inhibitors (e.g. thiazolidinedione) or miRNAs[38–42] **(Fig. 2g)**. Notably, somatotrophic
215 PitNETs from acromegalic patients highly expressed *CEBPD* **(Fig. 2g),** which actively represses other PIT1
216 lineage differentiations during normal development[11,43], suggesting that PitNETs may hijack inhibitory
217 mechanisms to dictate and maintain a specific hormonal phenotype. Additionally, we noted upregulation
218 of specific TF genes (e.g. *YBX3*, *SREBF1*, *ETV5*, *NPAS2*, and *TRPS1*) that have been implicated in the
219 pathogenesis of other neuroendocrine and non-neuroendocrine tumors, including colorectal,
220 nasopharyngeal, prostate, and breast cancers. **(Fig. 2g)**[44–48]. These findings lend support to the controversial
221 2022 WHO classification of pituitary tumors as encompassing features of both neuroendocrine and non-
222 neuroendocrine tumors [49].

223 We next compared the transcriptomes of secreting versus silent corticotrophic PitNETs given their
224 presumed origin from a common TPIT lineage cell. As expected, TPIT was equally present in both secreting
225 and silent corticotrophic PitNETs, and secreting corticotrophic PitNETs showed increased expression of
226 POMC **(Fig. 2h)**, a key precursor of ACTH absent in silent corticotrophic PitNETs**.** Surprisingly, and
227 consistent with our CNV findings, there were far more differences between secreting versus silent
228 corticotrophic PitNETs than just POMC loss in the latter, as we found secreting corticotrophic PitNETs to
229 be less mature and differentiated than silent corticotrophic PitNETs, with secreting corticotrophic PitNETs
230 displaying higher expression of genes involved in morphogenesis and cellular development compared to
231 silent corticotrophic PitNETs **(Fig. 2h)** and silent corticotrophic PitNETs expressing genes involved in
232 intracellular vesicular transport, localization, and synaptic release, indicating retained functional-structural
233 potential characteristic of a mature state **(Fig. 2h).** Silent corticotrophic PitNETs also had higher expression

234 of *PCSK1N*, an indirect inhibitor of ACTH maturation **(Fig. 2h)**, potentially actively repressing hormone
235 production in ways beyond their previously demonstrated loss of POMC expression.

236 The classification of NCAs and SGAs as distinct subgroups of nonfunctioning PitNETs is still a
237 subject of debate[37,50]. Our analysis reveals that despite being non-functioning, SGAs exhibit gene
238 expression patterns related to hormonal secretion, similar to SCAs. **(Fig. 2h)**. In contrast, NCAs exhibit
239 upregulation of genes involved in cell-cell adhesion and communication, indicating the presence of a robust
240 intercellular network akin to that found in normal neuroendocrine cells **(Fig. 2h).**

241

242 **2.3 Cellular trajectories of PitNET subtypes**

243 The cellular origin of PitNETs remains uncertain,[51–53] with two prevailing hypotheses. The first
244 hypothesis is that PitNETs originate from the oncogenic transformation of cells in the normal pituitary
245 gland with a stem-like transcriptome that we identified in our analysis of normal adult pituitary glands
246 above **(Fig. 1b, e)**. The second hypothesis is that PitNETs derive from differentiated neuroendocrine cells
247 in the normal gland that undergo clonal de-differentiation to produce a tumor-initiating stem-like cell with
248 an endocrine phenotype.[54] To identify the proximate precursor cells of each PitNET subtype, we conducted
249 pseudotime trajectory analysis using adult pituitary stem cells in the normal pituitary gland, mature
250 neuroendocrine cells in the normal pituitary gland, and PitNET cells **(Supplementary Table 4).**
251 Interestingly, we found that PitNETs exhibited both origin patterns depending on their subtype **(Fig. 3a-e)**.

252 Normal adult gonadotroph cells were intermediaries between normal stem cells and SGA tumor
253 cells, indicating the likely origin of SGAs from differentiated gonadotroph cells **(Fig. 3d)**. Similarly, all
254 lactotrophic PitNET cells emerged after normal mature lactotroph cells in the trajectory and were further
255 categorized into early-phase (Early-Prl) and late-phase (Late-Prl) **(Fig. 3c, f).** Early-Prl cells highly
256 expressed TF genes such as *ZNF91*, *CUX1*, *FOXK1*, *ESR1*, and *GATAD2B*, whereas Late-PRL cells
257 predominantly expressed *ZNF33B*, *MECOM*, *PITX1*, and *FOS* **(Fig. 3f, g)**. We also examined the
258 pseudotime ordering of Cushing's adenomas and SCA, based on our transcriptomic data suggesting a more
259 differentiated phenotype for SCA **(Fig. 2e)**. Both tumor types emerged after normal mature corticotroph

260 cells, and SCA emerged at a later stage than Cushing's adenomas **(Figure 3e),** supporting our earlier
261 findings **(Fig. 2h)**.

262 In contrast to these PitNET subtypes which appeared to arise from differentiated neuroendocrine
263 cells in the normal gland, somatrophic PitNET cells appear early in the trajectory from stem cells, prior to
264 normal mature somatotroph cells **(Fig. 3a)**, suggesting a close link with glandular stem cells rather than
265 mature endocrine cells. NCAs, which lack differentiation markers as indicated by IHC and specific lineage-
266 specific TFs, remain enigmatic in their origins, though they are occasionally speculated to be
267 gonadotrophic.[55] Our reconstructed pseudotime trajectory incorporating NCAs, stem cells, and all five types
268 of mature neuroendocrine cells shows that NCAs emerge early, immediately following normal stem cells
269 **(Fig. 3b)**, suggesting that their origins are more closely linked to normal stem cells, rather than any mature
270 endocrine cell types. Interestingly, both of these subtypes that appeared to originate from stem cells in the
271 normal pituitary gland (somatotrophic PitNETs and NCAs) also had the least CNV changes, a finding that
272 contrasts malignant cancers where cancers originating from cells with greater plasticity tend to be
273 associated with more CNV changes.[56,57]

274

275 **2.4 Cell-to-cell communication networks in the normal pituitary gland and in PitNETs**

276 Previous studies have speculated that the anterior lobe of the pituitary gland is not merely a
277 patchwork of hormone-secreting cells but rather a well-organized network capable of close-distance
278 crosstalk and co-oscillation, enabling a coordinated response to physiological stimuli[58–60]. Using CellChat[61],
279 we first identified 46 diverse cell-cell signaling pathways in the normal anterior lobe of the pituitary gland
280 based on ligand-receptor expressions. These pathways include NRG, NRXN, CADM, NCAM, VISFATIN,
281 ALCAM, PDGF, and VEGF signaling **(Fig. 4a, b; Supplementary Table 5).**

282 Subsequent unsupervised clustering revealed two distinct cell-cell communication patterns in the
283 normal anterior lobe of the pituitary gland: Pattern A, characterized by neuroendocrine cells communicating
284 with different subtypes of neuroendocrine cells via pathways associated with cell-cell adhesions and
285 junctions, suggesting their engagement in close communication networks and crosstalk[59,62]; and Pattern B,

286 consisting of non-neuroendocrine cells communicating with pituitary stem cells through pathways related
287 to immune, vascular, and other cellular functions **(Fig. 4c)**. Notably, within Pattern A, we identified the
288 ephrin-ephrin receptor signaling pathway, a subset of receptor tyrosine kinase capable of bidirectional
289 intercellular signaling. This pathway has been shown to play a crucial role in facilitating communication
290 between β cells of the pancreatic islets for glucose-insulin homoestasis[63,64], suggesting potential utilization
291 of this network broadly across organs within the endocrine system engaging in physiological homeostasis.
292 Interestingly, pan-hormonal cluster, emerging early in pseudotime **(Fig. 1d)**, lacked the typical pattern A
293 cell-cell communication characteristics seen in other neuroendocrine cell types and clustered closer to the
294 pattern B communication pattern seen with pituitary stem cells (**Fig. 4c)**, further indicating its incompletely
295 differentiated and highly plastic state.

296 We next examined if PitNET tumor cells retain these communication pathways we had identified
297 for cells in the normal pituitary gland **(Fig. 4d).** Surprisingly, PitNET cells closely mirrored normal
298 neuroendocrine cell signaling, with high expression of pathways like NRG, NRXN, NEGR, and CNTN.
299 EPHA was also highly expressed in pituitary tumor cells, except in Cushing's and SCA cells **(Fig. 4d).**
300 These findings suggest that PitNET cells utilize many examples of the two patterns of cell-to-cell
301 communication we had identified in normal pituitary cells, and we speculate that close communication
302 networks[65] may be crucial for tumor cell survival and growth.

303

304 **2.5 PitNET microenvironment**

305 The tumor microenvironment is a highly structured ecosystem, consisting of tumor cells surrounded
306 by diverse cell types and often embedded within an altered, vascularized extracellular matrix[6,66,67]. Our
307 PitNET samples predominantly consisted of tumor cells, but we also detected various non-tumor cells,
308 including normal neuroendocrine cells (corticotrophs, gonadotrophs, lactotrophs, and somatotrophs),
309 endothelial cells, pituicytes, macrophages, mixed stroma cells, and stem cells. Plurihormonal cells,
310 including pan-hormonal (i.e., cells with a somatotroph/lactotroph/corticotroph/gonadotroph signature),
311 were also present in the PitNETs. We first characterized TF and non-TF DEGs in the non-tumor cells **(Fig.**

312 **5a)** and then examined subtle transcriptomic differences between non-tumor cells in PitNET samples and
313 matched normal cell types in control samples **(Fig. 5b-l; Supplementary Table 6)**. Overall, normal
314 neuroendocrine cells in PitNETs had more downregulated genes compared to matched cell types in control
315 samples, except in lactotroph PitNETs, whose normal neuroendocrine cells exhibited more upregulated
316 genes compared to control samples **(Fig. 5i-l).** Similarly, pan-hormonal, macrophages, endothelial cells,
317 and stem cells all exhibited more downregulated genes in PitNETs compared to matched cell types in
318 control samples **(Fig. 5b-h)**, consistent with reports in which benign tumor cells will downregulate genes
319 in stromal cells to eliminate gene expression patterns from stroma that could suppress tumor growth while
320 malignant tumor cells will upregulate genes in the stroma to cause the stroma to actively support tumor
321 growth[68]**.** Intriguingly, gene ontology enrichment analysis identified a loss of protein translation at the pre-
322 synapse, synapse, and post-synapse as most significant findings across all normal monohormonal cells in
323 tumor samples **(Fig. 5b-h, Supplemental Table s6),** indicating these cells are compromised in maintaining
324 cellular connections, unlike in control samples where such networks are typically intact and functional **(Fig.**
325 **4d)**, suggesting that the loss of cell cohesiveness that neuropathologists describe as a defining characteristic
326 of PitNETs[69] is not just found in PitNET tumor cells but in the normal glandular cells in close proximity to
327 them. Additionally, macrophages in tumor samples exhibited a general loss of regulation of immune system
328 processes and leukocytic activation **(Fig. 5e, Supplementary Table 7)**, suggesting that tumor-associated
329 macrophages in PitNETs are in an immunosuppressed state.

330 To characterize the vascular microenvironment of PitNETs, we identified areas of high and low
331 vasculature density in PitNET paraffin slides and conducted spatial transcriptomic analysis **(Fig. 5m-q).**
332 This revealed 15 upregulated DEGs in PitNET cells surrounding highly vascularized areas compared to
333 those in low vascularized regions **(Fig. 5n),** including genes *COL4A2*, *RGS5*, *COL4A1*, *MYL9*, *HSPG2*,
334 *NOTCH3*, *VIM*, *IGFBP7*, *BGN*, *SPARC*, *FN1*, *PLVAP*, *IFITM3*, *EPAS1*, and *EGFL7*. Many of these genes
335 are associated with pro-angiogenic and tumorigenic activities[70–73]. Notably, *VIM* enhances tumor
336 malignancy through its role in epithelial-mesenchymal transition (EMT) and is a target for anti-angiogenic
337 immunotherapy[74]. Our findings suggest that crosstalk between PitNET cells and their local vasculature may

338 mediate specific transcriptomic alterations in PitNET cells, making these cells more tumorigenic than those
339 that do not interact with vessels, capturing a spatial-dependent heterogeneity within PitNETs beyond the
340 interactions identified from scRNA or snRNA data.
341
342 **3. Discussion**
343 Pituitary neuroendocrine tumors (PitNETs) represent a unique convergence of developmental
344 biology and oncogenesis, where the gland's inherent plasticity is co-opted to drive tumor heterogeneity.
345 Leveraging single-nuclei RNA sequencing (snRNA-seq) and spatial transcriptomics, we decode this
346 complexity, revealing PitNETs not as monolithic entities but as dynamic ecosystems shaped by lineage
347 fluidity and microenvironmental crosstalk. This plasticity-driven heterogeneity challenges the current
348 WHO classification framework—anchored in static lineage markers such as PIT1, TPIT, and SF1—and
349 repositions these tumors along a transcriptomic continuum where lineage boundaries are fluid and context-
350 dependent, necessitating a revised diagnostic paradigm.
351 Central to our findings is the identification of plurihormonal neuroendocrine cells in both normal
352 and neoplastic pituitary tissues. The persistence of these cells in PitNETs suggests that developmental
353 plasticity is not merely a vestige of normal differentiation but a possible driver of tumorigenesis. In the
354 normal adult pituitary gland, such plasticity likely facilitates adaptive responses to physiological demands,
355 such as lactation or stress. In tumors, however, these cells—which originate early in pseudotime trajectories,
356 retain stem-like transcriptional programs, and acquire hormonal signatures—are co-opted to sustain
357 transcriptional diversity. These unique characteristics may enable tumor cells to evade lineage-targeted
358 therapies and tumor suppression mechanisms.
359 Our trajectory analysis reveals two distinct oncogenic pathways in PitNETs: stem cell-derived
360 tumors (e.g., somatotroph and null cell adenomas) and differentiated-cell-derived tumors (e.g.,
361 prolactinomas and corticotroph adenomas). Strikingly, pituitary stem-derived tumors exhibit fewer somatic
362 copy-number alterations (CNAs) despite their primitive state—a paradox when contrasted with
363 malignancies like gliomas, where cancer stem cells drive hypermutant aggression[75]. This dichotomy

364 suggests that, in contrast to the genomic instability of cancer stem cells which have likely lost some capacity
365 for mutational correction, pituitary stem cell-derived PitNETs may retain the developmental checkpoints
366 found within pituitary stem cells[76] to balance proliferation and differentiation, mirroring the genomic
367 stability of fetal pituitary progenitors. In contrast, differentiated-cell-derived tumors may accumulate CNAs
368 under chronic secretory stress, reflecting a trade-off between hormonal hyperactivity and genomic fidelity.
369 These observations hint at a broader principle: PitNETs may occupy a middle ground between benign self-
370 limited growth and aggressive transformation, offering a model to study how tumors evolve within
371 constrained microenvironments.

372 PitNETs co-opt the pituitary's native communication networks, repurposing key signaling
373 pathways to promote tumor growth and survival. For instance, Ephrin signaling**,** essential for pulsatile
374 hormone secretion in the healthy pituitary, may be hijacked to synchronize proliferation and immune
375 evasion. Our CellChat analysis also identifies conserved ligand-receptor interactions, such as paracrine
376 growth factor NRG1-ERBB4**,** which play roles in synaptic plasticity and cytoarchitecture remodeling[77]. By
377 mimicking the normal pituitary's intrinsic ability to coordinate complex cellular functions, these tumors
378 may form self-organized collectives that evade immune responses and resist single-target therapies,
379 emphasizing the need for therapeutic approaches that target broader signaling networks.

380 Furthermore, spatial transcriptomics localizes PitNET tumor cell-stroma crosstalk to perivascular
381 niches. There is converging evidence that the tumor vasculature may function as a central hub to promote
382 cancer stemness, and thereby stimulate tumor growth independently of its role as a supplier of oxygen and
383 nutrients[78]. This observation has given rise to the term perivascular niche which refers to a
384 microenvironment generated by endothelial cells and mural cells that surround and support blood vessels,
385 along with nonvascular cells such as fibroblasts. In a variety of cancers, the perivascular niche affects the
386 behavior of adjacent tumor cells, including by promoting their stemness. In the case of PitNETs, spatial
387 transcriptomics revealed that tumor cells in the perivascular niche upregulate pro-angiogenic factors and
388 EMT inducers, reflecting the bidirectional signaling that occurs between tumor cells and vascular cells in
389 the perivascular niche. Tumor cells within these perivascular niches also upregulate matrix proteins (i.e.,

390 COL4A1, FN1), generating a provisional vessel-adjacent scaffold that could foster perivascular invasion—
391 a mechanism previously described in metastatic carcinomas[79,80] but less well-documented in benign
392 neoplasms. Together, these findings reveal how PitNETs exploit both developmental signaling and stromal
393 remodeling.

394 While our study provides important insights into PitNET biology, several limitations warrant
395 consideration. First, despite analyzing the largest snRNA-seq dataset to date, rare PitNET subtypes (e.g.,
396 thyrotroph tumors) remain underrepresented, potentially obscuring subtype-specific mechanisms. Second,
397 our findings implicating developmental plasticity and stromal crosstalk in tumorigenesis are primarily
398 correlative; functional validation in *in vivo* models is needed to establish causality. Finally, our use of
399 transcriptomic data may overlook post-transcriptional regulatory mechanisms, including alternative
400 splicing, which could provide deeper insights into tumor heterogeneity[7]. Addressing these limitations in
401 future studies will refine our understanding of PitNET heterogeneity and accelerate therapeutic translation.

402 Our work redefines PitNETs as ecosystems shaped by developmental plasticity and
403 microenvironmental hijacking. As a gland central to physiological homeostasis, it is fitting that its tumors
404 exhibit a biology as adaptable and interdependent as the systems they disrupt. These insights may extend
405 beyond PitNETs, offering a framework to investigate lineage fluidity and niche dependencies in other
406 endocrine neoplasms where similar mechanisms may take place.

407

408 **4. Methods**

409 **Human Tissue Procurement**

410 Pituitary tumor samples (n = 11) were obtained from patients who underwent transsphenoidal endoscopic
411 surgery at the University of California, San Francisco (UCSF) Department of Neurosurgery between 2022
412 and 2023. Non-tumor pituitary samples (n = 2) were acquired from UCSF Neurodegenerative Disease Brain
413 Bank autopsies in 2023 with a postmortem interval of less than 10 hours. Final neuropathology diagnoses
414 were 1) no disease and 2) Alzheimer's disease. All tissues were snap-frozen in -80 degrees Celsius
415 immediately upon collection. Tumor samples were histologically stained and pathologically diagnosed

416 using standard WHO criteria. All procedures were approved by the UCSF Institutional Review Board (IRB)
417 for human tissue research.

418 **Nuclei Isolation**

419 For snRNA-seq, nuclei were extracted from frozen tissues using the 'Van Helsing' protocol (Martelotto, L.,
420 Centre for Cancer Research, Victorian Comprehensive Cancer Centre; protocol available at 10x Genomics
421 dx.doi.org/10.17504/protocols.io.bdeni3de). Frozen tissues were mechanically dissociated in 500 µL lysis
422 buffer (Nuclei EZ Lysis Buffer, MilliporeSigma) using a Dounce homogenizer. Lysates were filtered
423 through a 30-µm strainer, pelleted, washed in nuclei wash buffer (10x Genomics), and stained with Vybrant
424 DyeCycle Ruby Stain (Fisher Scientific) for sorting on a Sony SH800 sorter.

425 **SnRNA cDNA Library Generation**

426 Isolated nuclei were resuspended in cold DPBS containing 1% BSA and 0.5 U/µL RNase inhibitor (Thomas
427 Scientific, #C756R82). After sorting, 15,000 nuclei per sample were loaded into 10x Genomics capture
428 reactions. Libraries were prepared using the Chromium Next GEM Single Cell 3′ Reagent Kit v3.1 (Dual
429 Index, 10x Genomics, #CG000315) following the manufacturer's protocol. Sequencing was performed on
430 an Illumina NovaSeq with recommended parameters (28 × 10 × 10 × 90 cycles).

431 **SnRNA Data Processing**

432 Raw sequencing data were processed using 10x Genomics' Cell Ranger Count (v7.0.1) on the 10x
433 Genomics Cloud Analysis platform. Cell/feature matrices were imported into RStudio and converted to
434 Seurat objects (v4.2.0). Low-quality cells and doublets were filtered by excluding outliers with extreme
435 gene counts or mitochondrial contamination (>5%). After preprocessing, mitochondrial RNA accounted
436 for 0.25% ± 0.71% (mean ± SD) of nuclear RNA. Data were log-normalized, scaled, and integrated using
437 canonical correlation analysis (CCA) to mitigate batch effects. Clustering resolutions (0–1.5, increments of
438 0.1) were optimized to maximize cluster distinctiveness while minimizing nucleus reassignment.
439

440 **Cluster Annotation**

441 Cluster annotation was performed via consensus across three independent methods to ensure labeling
442 accuracy. First, label transfer was conducted using the SingleR package, referencing both the standard
443 human atlas and the Darmanis brain atlas. Second, canonical pituitary cell markers were used to compute
444 module scores for each cluster. Finally, tumor nuclei were co-embedded with a normal pituitary snRNA-
445 seq atlas (derived from two control samples) to validate cluster identities. Annotations were assigned based
446 on concordance across methods and the confidence scores of each labeling approach.

447

448 **Pseudobulk and Copy Number Variation (CNV) Analysis**

449 Pseudobulk transcriptomes were hierarchically clustered by Euclidean distance. CNVs were inferred using
450 InferCNV (v1.14.2), comparing tumor nuclei to non-tumor controls. Tumors were reclustered by CNV
451 magnitude and genomic location.

452

453 **Differential Gene Expression and Ontology Analysis**

454 Differentially expressed genes (DEGs) were identified using Seurat's FindMarkers (Wilcoxon test,
455 Bonferroni-adjusted $p < 0.05$). Results were visualized via DotPlots (Seurat) and EnhancedVolcano
456 (v1.16.0). Gene ontology was performed using ToppGene.

457

458 **Trajectory Analysis**

459 Monocle (v2.26.0) reconstructed pseudotime trajectories for stem/neuroendocrine nuclei. Stem cells were
460 designated as root notes. Pseudotime-correlated DEGs were cross-referenced with cluster markers, and
461 ontology analysis identified pathways linked to tumorigenesis. Prolactinomas were stratified into early/late
462 pseudotime states for phase-specific DEG analysis.

463

464 **Cell-Cell Communication Analysis**

465 CellChat (v1.6.1) inferred ligand-receptor interactions using the reference CellChatDB.human. Pathway
466 activity was quantified by ligand-receptor co-expression, and cluster-specific networks were computed.
467 Signaling pathways were clustered by interaction similarity, and cell clusters were meta-clustered based on
468 communication patterns.

469 **Spatial Transcriptomics Tissue Preparation and Staining**

470 Frozen pituitary adenomas were thawed, fixed in 4% paraformaldehyde, paraffin-embedded, and sectioned
471 at 5 μm thickness. Deparaffinized slides underwent spatial whole-transcriptome profiling on the GeoMx
472 Digital Spatial Profiler (DSP)(Bruker NanoStrings). Antigen retrieval (20 minutes) and Proteinase K
473 digestion (0.1 mg/mL, 15 minutes) preceded staining with AF532-conjugated anti-CD68 (1:100, Novus,
474 #NBP2-34587AF532), AF647-conjugated anti-α-smooth muscle actin (αSMA; 1:200, Novus, #NBP2-
475 3522AF647), and SYTO13 nuclear dye (1:10, Bruker).

476 **Spatial Transcriptomics Imaging and Analysis**

477 Morphology marker images were acquired using FITC (30 ms exposure), Cy3 (300 ms), and Cy5 (300 ms)
478 fluorescence channels. Regions of interest (ROIs) were selected based αSMA+ and αSMA- expression for
479 spatially resolved transcript capture. Raw sequencing data were normalized to the geometric mean of
480 housekeeping gene expression levels and analyzed using GeoMx Digital Spatial Profiler (DSP) software.
481 Differentially expressed genes (DEGs) were defined by a Benjamini–Hochberg $FDR < 0.05$ and $|\log2(\text{fold change})| > 0.5$.

483

484 **5. Acknowledgements**

485 The authors thank the study participants at the University of California, San Francisco, for their valuable
486 tissue donations. They also acknowledge the staff and study coordinators at the UCSF Brain Tumor Center
487 and Neurodegenerative Disease Brain Bank. This research was supported by the following funding sources:
488 NIH 1R01CA227136 (M.K.A.) , 2R01NS079697 (M.K.A.), 1R01NS123808 (M.K.A.), UCSF Resource

Allocation Program (M.K.A.), P30 AG062422 (L.T.G.), K24 AG053435 (L.T.G.), and the Milky Way Research Foundation (P.G.)

6. Contributions

R.C.O., J.Y.O., J.J. contributed equally as co-first authors. R.C.O., J.Y.O., J.J. and M.K.A. designed the study. R.C.O., J.Y.O., J.J. performed single-nuclei RNA-sequencing experiments and data analysis with significant contributions from A.S., M.L., and H.K.. A.J.E., N.B., and P.G. performed spatial transcriptomics experiments and data analysis. W.W.S., L.T.G., and A.D. contributed to critical data collection and interpretation. R.C.O., J.Y.O., J.J. wrote the manuscript, and all authors contributed to the writing and provided comments. M.K.A. provided supervision.

512 **REFERENCES**

513

514 1. Mete, O. & Lopes, M. B. Overview of the 2017 WHO Classification of Pituitary Tumors. *Endocr*
515 *Pathol* **28**, 228–243 (2017).
516 2. Asa, S. L., Mete, O., Perry, A. & Osamura, R. Y. Overview of the 2022 WHO Classification of
517 Pituitary Tumors. *Endocr Pathol* **33**, 6–26 (2022).
518 3. Zhang, Q. *et al.* Single-cell sequencing identifies differentiation-related markers for molecular
519 classification and recurrence prediction of PitNET. *Cell Reports Medicine* **4**, 100934 (2023).
520 4. Neou, M. *et al.* Pangenomic Classification of Pituitary Neuroendocrine Tumors. *Cancer Cell* **37**, 123-
521 134.e5 (2020).
522 5. Cui, Y. *et al.* Single-cell transcriptome and genome analyses of pituitary neuroendocrine tumors.
523 *Neuro-Oncology* **23**, 1859–1871 (2021).
524 6. Yan, N. *et al.* Single-cell transcriptomic analysis reveals tumor cell heterogeneity and immune
525 microenvironment features of pituitary neuroendocrine tumors. *Genome Medicine* **16**, 2 (2024).
526 7. Huang, Y. *et al.* Splicing diversity enhances the molecular classification of pituitary neuroendocrine
527 tumors. *Nat Commun* **16**, 1552 (2025).
528 8. Slyper, M. *et al.* A single-cell and single-nucleus RNA-Seq toolbox for fresh and frozen human
529 tumors. *Nat Med* **26**, 792–802 (2020).
530 9. Habib, N. *et al.* Massively-parallel single nucleus RNA-seq with DroNc-seq. *Nat Methods* **14**, 955–
531 958 (2017).
532 10. Hao, Y. *et al.* Integrated analysis of multimodal single-cell dat. Preprint at
533 https://doi.org/10.1101/2020.10.12.335331 (2020).
534 11. Zhang, S. *et al.* Single-cell transcriptomics identifies divergent developmental lineage trajectories
535 during human pituitary development. *Nat Commun* **11**, 5275 (2020).
536 12. Aran, D. *et al.* Reference-based analysis of lung single-cell sequencing reveals a transitional
537 profibrotic macrophage. *Nat Immunol* **20**, 163–172 (2019).

538 13. Cheung, L. Y. M. *et al.* Single-Cell RNA Sequencing Reveals Novel Markers of Male Pituitary Stem
539 Cells and Hormone-Producing Cell Types. *Endocrinology* **159**, 3910–3924 (2018).
540 14. Russell, J. P. *et al.* Pituitary stem cells produce paracrine WNT signals to control the expansion of
541 their descendant progenitor cells. *Elife* **10**, e59142 (2021).
542 15. Rizzoti, K., Akiyama, H. & Lovell-Badge, R. Mobilized adult pituitary stem cells contribute to
543 endocrine regeneration in response to physiological demand. *Cell Stem Cell* **13**, 419–432 (2013).
544 16. Zhang, Z. *et al.* Single nucleus transcriptome and chromatin accessibility of postmortem human
545 pituitaries reveal diverse stem cell regulatory mechanisms. *Cell Reports* **38**, 110467 (2022).
546 17. Frawley, L. S. & Boockfor, F. R. Mammosomatotropes: Presence and Functions in Normal and
547 Neoplastic Pituitary Tissue*. *Endocrine Reviews* **12**, 337–355 (1991).
548 18. Shi, R. *et al.* Clinicopathological Characteristics of Plurihormonal Pituitary Adenoma. *Front Surg* **9**,
549 826720 (2022).
550 19. Scheithauer, B. W. *et al.* Plurihormonal pituitary adenomas. *Semin Diagn Pathol* **3**, 69–82 (1986).
551 20. Mete, O., Alshaikh, O. M., Cintosun, A., Ezzat, S. & Asa, S. L. Synchronous Multiple Pituitary
552 Neuroendocrine Tumors of Different Cell Lineages. *Endocr Pathol* **29**, 332–338 (2018).
553 21. Mitrofanova, L. B., Konovalov, P. V., Krylova, J. S., Polyakova, V. O. & Kvetnoy, I. M.
554 Plurihormonal cells of normal anterior pituitary: Facts and conclusions. *Oncotarget* **8**, 29282–29299
555 (2017).
556 22. Denef, C., Pals, K., Hauspie, A., Vankelecom, H. & Seuntjens, E. Combinatorial Expression of
557 Phenotypes of Different Cell Lineages in the Rat and Mouse Pituitary. *Annals of the New York*
558 *Academy of Sciences* **1040**, 84–88 (2005).
559 23. Seuntjens, E., Hauspie, A., Vankelecom, H. & Denef, C. Ontogeny of Plurihormonal Cells in the
560 Anterior Pituitary of the Mouse, as Studied by Means of Hormone mRNA Detection in Single Cells.
561 *Journal of Neuroendocrinology* **14**, 611–619 (2002).
562 24. Villalobos, C., Núñez, L. & García-Sancho, J. Anterior pituitary thyrotropes are multifunctional cells.
563 *American Journal of Physiology-Endocrinology and Metabolism* **287**, E1166–E1170 (2004).

564 25. Van den Berge, K. *et al.* Trajectory-based differential expression analysis for single-cell sequencing
565 data. *Nat Commun* **11**, 1201 (2020).
566 26. Hou, W. *et al.* A statistical framework for differential pseudotime analysis with multiple single-cell
567 RNA-seq samples. *Nat Commun* **14**, 7286 (2023).
568 27. Le Tissier, P. R., Murray, J. F. & Mollard, P. A New Perspective on Regulation of Pituitary Plasticity:
569 The Network of SOX2-Positive Cells May Coordinate Responses to Challenge. *Endocrinology* **163**,
570 bqac089 (2022).
571 28. Ho, Y. *et al.* Single-cell transcriptomic analysis of adult mouse pituitary reveals sexual dimorphism
572 and physiologic demand-induced cellular plasticity. *Protein Cell* **11**, 565–583 (2020).
573 29. Childs, G. V., MacNicol, A. M. & MacNicol, M. C. Molecular Mechanisms of Pituitary Cell
574 Plasticity. *Frontiers in Endocrinology* **11**, (2020).
575 30. Friend, K. E. *et al.* Estrogen receptor expression in human pituitary: correlation with
576 immunohistochemistry in normal tissue, and immunohistochemistry and morphology in
577 macroadenomas. *J Clin Endocrinol Metab* **78**, 1497–1504 (1994).
578 31. Peel, M. T., Ho, Y. & Liebhaber, S. A. Transcriptome Analyses of Female Somatotropes and
579 Lactotropes Reveal Novel Regulators of Cell Identity in the Pituitary. *Endocrinology* **159**, 3965–3980
580 (2018).
581 32. Holla, V. R., Mann, J. R., Shi, Q. & DuBois, R. N. Prostaglandin E2 regulates the nuclear receptor
582 NR4A2 in colorectal cancer. *J Biol Chem* **281**, 2676–2682 (2006).
583 33. Kim, K.-S. *et al.* Orphan nuclear receptor Nurr1 directly transactivates the promoter activity of the
584 tyrosine hydroxylase gene in a cell-specific manner. *J Neurochem* **85**, 622–634 (2003).
585 34. Cooper, O. *et al.* Silent corticogonadotroph adenomas: clinical and cellular characteristics and long-
586 term outcomes. *Horm Cancer* **1**, 80–92 (2010).
587 35. Bi, W. L. *et al.* Landscape of Genomic Alterations in Pituitary Adenomas. *Clinical Cancer Research*
588 **23**, 1841–1851 (2017).

589 36. Lasolle, H. *et al.* Chromosomal instability in the prediction of pituitary neuroendocrine tumors
590 prognosis. *Acta Neuropathologica Communications* **8**, 190 (2020).
591 37. Pangenomic Classification of Pituitary Neuroendocrine Tumors: Cancer Cell.
592 https://www.cell.com/cancer-cell/fulltext/S1535-6108(19)30522-7#secsectitle0075.
593 38. Heaney, A. P., Fernando, M. & Melmed, S. PPAR-γ receptor ligands: novel therapy for pituitary
594 adenomas. *J Clin Invest* **111**, 1381–1388 (2003).
595 39. Zhan, X., Li, J. & Zhou, T. Targeting Nrf2-Mediated Oxidative Stress Response Signaling Pathways
596 as New Therapeutic Strategy for Pituitary Adenomas. *Front Pharmacol* **12**, 565748 (2021).
597 40. Zhan, X. & Desiderio, D. M. Signaling pathway networks mined from human pituitary adenoma
598 proteomics data. *BMC Medical Genomics* **3**, 13 (2010).
599 41. Renjie, W. & Haiqian, L. MiR-132, miR-15a and miR-16 synergistically inhibit pituitary tumor cell
600 proliferation, invasion and migration by targeting Sox5. *Cancer Lett* **356**, 568–578 (2015).
601 42. Srirangam Nadhamuni, V. & Korbonits, M. Novel Insights into Pituitary Tumorigenesis: Genetic and
602 Epigenetic Mechanisms. *Endocr Rev* **41**, 821–846 (2020).
603 43. Tong, Y. *et al.* CEBPD Suppresses Prolactin Expression and Prolactinoma Cell Proliferation. *Mol*
604 *Endocrinol* **25**, 1880–1891 (2011).
605 44. Peng, Y. *et al.* The role of E26 transformation-specific variant transcription factor 5 in colorectal
606 cancer cell proliferation and cell cycle progression. *Cell Death Dis* **12**, 1–11 (2021).
607 45. Fan, X. *et al.* YBX3 Mediates the Metastasis of Nasopharyngeal Carcinoma via PI3K/AKT Signaling.
608 *Front. Oncol.* **11**, (2021).
609 46. Li, L.-Y. *et al.* Interplay and cooperation between SREBF1 and master transcription factors regulate
610 lipid metabolism and tumor-promoting pathways in squamous cancer. *Nat Commun* **12**, 4362 (2021).
611 47. Ma, S. *et al.* NPAS2 promotes aerobic glycolysis and tumor growth in prostate cancer through HIF-1A
612 signaling. *BMC Cancer* **23**, 280 (2023).
613 48. Elster, D. *et al.* TRPS1 shapes YAP/TEAD-dependent transcription in breast cancer cells. *Nat*
614 *Commun* **9**, 3115 (2018).

615 49. The World Health Organization classifications of pituitary neuroendocrine tumours: a clinico-
616 pathological appraisal in: Endocrine-Related Cancer Volume 30 Issue 8 (2023).
617 https://erc.bioscientifica.com/view/journals/erc/30/8/ERC-23-0021.xml.
618 50. Haddad, A. F. *et al.* Clinical characteristics and outcomes of null-cell versus silent gonadotroph
619 adenomas in a series of 1166 pituitary adenomas from a single institution. *Neurosurgical Focus* **48**,
620 E13 (2020).
621 51. Sox2+ Stem/Progenitor Cells in the Adult Mouse Pituitary Support Organ Homeostasis and Have
622 Tumor-Inducing Potential: Cell Stem Cell. https://www.cell.com/cell-stem-cell/fulltext/S1934-
623 5909(13)00312-
624 3?_returnURL=https%3A%2F%2Flinkinghub.elsevier.com%2Fretrieve%2Fpii%2FS19345909130031
625 23%3Fshowall%3Dtrue.
626 52. Yuan, L. *et al.* Identification and gene expression profiling of human gonadotrophic pituitary adenoma
627 stem cells. *Acta Neuropathologica Communications* **11**, 24 (2023).
628 53. Oh, J. Y. *et al.* Transcriptomic Profiles of Normal Pituitary Cells and Pituitary Neuroendocrine Tumor
629 Cells. *Cancers* **15**, 110 (2023).
630 54. The clonal origin and clonal evolution of epithelial tumours - PMC.
631 https://www.ncbi.nlm.nih.gov/pmc/articles/PMC2517717/.
632 55. Kontogeorgos, G. & Thodou, E. The gonadotroph origin of null cell adenomas. *Hormones (Athens)*
633 **15**, 243–247 (2016).
634 56. Wei, G., Zhang, X., Liu, S., Hou, W. & Dai, Z. Comprehensive data mining reveals RTK/RAS
635 signaling pathway as a promoter of prostate cancer lineage plasticity through transcription factors and
636 CNV. *Sci Rep* **14**, 11688 (2024).
637 57. Dai, Z. & Liu, P. High copy number variations, particular transcription factors, and low immunity
638 contribute to the stemness of prostate cancer cells. *J Transl Med* **19**, 206 (2021).
639 58. Mollard, P., Hodson, D. J., Lafont, C., Rizzoti, K. & Drouin, J. A tridimensional view of pituitary
640 development and function. *Trends in Endocrinology & Metabolism* **23**, 261–269 (2012).

641 59. Le Tissier, P. R. *et al.* Anterior pituitary cell networks. *Frontiers in Neuroendocrinology* **33**, 252–266
642 (2012).
643 60. Hodson, D. J. *et al.* Existence of long-lasting experience-dependent plasticity in endocrine cell
644 networks. *Nat Commun* **3**, 605 (2012).
645 61. Jin, S. *et al.* Inference and analysis of cell-cell communication using CellChat. *Nat Commun* **12**, 1088
646 (2021).
647 62. Denef, C. Paracrinicity: The Story of 30 Years of Cellular Pituitary Crosstalk. *Journal of*
648 *Neuroendocrinology* **20**, 1–70 (2008).
649 63. Kulkarni, R. N. & Kahn, C. R. Ephs and Ephrins Keep Pancreatic β Cells Connected. *Cell* **129**, 241–
650 243 (2007).
651 64. Konstantinova, I. *et al.* EphA-Ephrin-A-mediated beta cell communication regulates insulin secretion
652 from pancreatic islets. *Cell* **129**, 359–370 (2007).
653 65. Su, J. *et al.* Cell–cell communication: new insights and clinical implications. *Sig Transduct Target*
654 *Ther* **9**, 1–52 (2024).
655 66. Lin, S. *et al.* Single-cell transcriptomics reveal distinct immune-infiltrating phenotypes and
656 macrophage–tumor interaction axes among different lineages of pituitary neuroendocrine tumors.
657 *Genome Medicine* **16**, 60 (2024).
658 67. Lyu, L. *et al.* Single-cell sequencing of PIT1-positive pituitary adenoma highlights the pro-tumour
659 microenvironment mediated by IFN-γ-induced tumour-associated fibroblasts remodelling. *Br J Cancer*
660 **128**, 1117–1133 (2023).
661 68. Amini, P., Nassiri, S., Malbon, A. & Markkanen, E. Differential stromal reprogramming in benign and
662 malignant naturally occurring canine mammary tumours identifies disease-modulating stromal
663 components. *Sci Rep* **10**, 5506 (2020).
664 69. Mete, O. & Asa, S. L. Clinicopathological correlations in pituitary adenomas. *Brain Pathol* **22**, 443–
665 453 (2012).

666 70. Gao, Z. *et al.* SPARC Overexpression Promotes Liver Cancer Cell Proliferation and Tumor Growth.
667 *Front. Mol. Biosci.* **8**, (2021).
668 71. Berr, A. L. *et al.* Vimentin is required for tumor progression and metastasis in a mouse model of non–
669 small cell lung cancer. *Oncogene* **42**, 2074–2087 (2023).
670 72. Wang, Y. *et al.* EGFL7 drives the evolution of resistance to EGFR inhibitors in lung cancer by
671 activating NOTCH signaling. *Cell Death Dis* **13**, 1–15 (2022).
672 73. Deng, S. *et al.* MYL9 expressed in cancer-associated fibroblasts regulate the immune
673 microenvironment of colorectal cancer and promotes tumor progression in an autocrine manner.
674 *Journal of Experimental & Clinical Cancer Research* **42**, 294 (2023).
675 74. van Beijnum, J. R. *et al.* Extracellular vimentin mimics VEGF and is a target for anti-angiogenic
676 immunotherapy. *Nat Commun* **13**, 2842 (2022).
677 75. Chu, X. *et al.* Cancer stem cells: advances in knowledge and implications for cancer therapy. *Sig*
678 *Transduct Target Ther* **9**, 1–63 (2024).
679 76. Pérez Millán, M. I. *et al.* Pituitary stem cells: past, present and future perspectives. *Nat Rev*
680 *Endocrinol* **20**, 77–92 (2024).
681 77. Mei, L. & Nave, K.-A. Neuregulin-ERBB signaling in the nervous system and neuropsychiatric
682 diseases. *Neuron* **83**, 27–49 (2014).
683 78. Nowosad, A., Marine, J.-C. & Karras, P. Perivascular niches: critical hubs in cancer evolution. *Trends*
684 *Cancer* **9**, 897–910 (2023).
685 79. Li, B. *et al.* Fibronectin 1 promotes melanoma proliferation and metastasis by inhibiting apoptosis and
686 regulating EMT. *Onco Targets Ther* **12**, 3207–3221 (2019).
687 80. Wang, T. *et al.* COL4A1 promotes the growth and metastasis of hepatocellular carcinoma cells by
688 activating FAK-Src signaling. *Journal of Experimental & Clinical Cancer Research* **39**, 148 (2020).
689
690
691

692 **FIGURES**

693

694 **Figure 1: Study overview and single-nucleus transcriptomic atlas of the normal human pituitary**. (**a**)
695 Overview of study cohort and tissue samples. (**b**) Dimensional reduction plot of human pituitary gland
696 nuclei, clustered by cell identity. (**c**) Dimensional reduction plot of human pituitary gland nuclei, clustered
697 by patient origin of tissue sample. (**d**) Stacked bar chart of relative cluster sizes in each normal control
698 sample. (**e**) Transcriptomic heatmap of RNA expression of canonical markers expressed in the adult
699 pituitary gland. (**f**) Dimensional reduction plot of human pituitary gland nuclei after trajectory analysis,
700 colored by pseudotime. (**g**) Ridge plot of normal pituitary clusters demonstrating pseudotime distribution
701 of each cluster and ordered by mean pseudotime. TF: transcription factor.

702

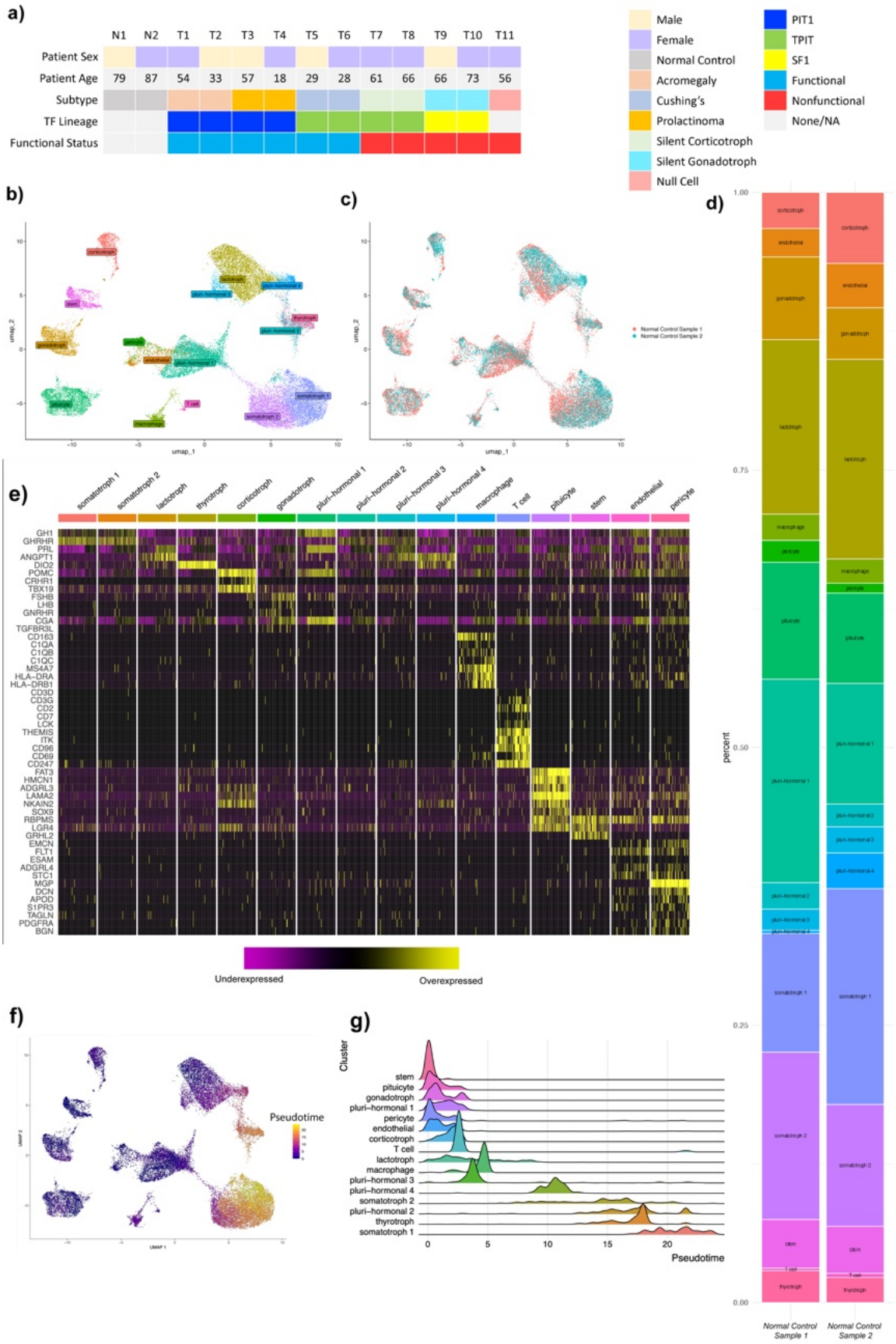
a)
N1 N2 T1 T2 T3 T4 T5 T6 T7 T8 T9 T10 T11
Patient Sex
Patient Age 79 87 54 33 57 18 29 28 61 66 66 73 56
Subtype
TF Lineage
Functional Status
Male
Female
Normal Control
Acromegaly
Cushing's
Prolactinoma
Silent Corticotroph
Silent Gonadotroph
Null Cell
PIT1
TPIT
SF1
Functional
Nonfunctional
None/NA
b)
c)
d)
e)
Underexpressed
Overexpressed
f)
Pseudotime
g)
Cluster
Pseudotime
percent
Normal Control Sample 1
Normal Control Sample 2

703

704 **Figure 2**: **Transcriptomic and copy number variation (CNV) analysis of pituitary neuroendocrine**
705 **tumors.** (**a**) Dimensional reduction plot of pituitary neuroendocrine tumors and nontumor nuclei from all
706 samples, integrated and clustered by tumor subtype vs nontumor status. (**b**) Dimensional reduction plot of
707 pituitary neuroendocrine tumors and nontumor nuclei from all samples, further subclustered to display the
708 identities of nontumor nuclei. (**c**) Clustering of nuclei based on tumor subtype and nontumor status, based
709 on overall pseudobulk transcriptomic expression. (**d**) Relative contributions and locations of each tumor
710 subtype to the overall dimensional reduction (upper), followed by CNV analysis of each tumor subtype
711 relative to nontumor controls (lower). (**e**) Heatmap of aggregated CNV data, plotting relative percent of
712 genes altered per chromosome and split by tumor subtype vs normal control. Ordered by chromosome
713 number and CNV gain vs loss. (**f**) Heatmap of aggregated CNV data, clustered by similar CNV expression.
714 (**g**) Transcription factor analysis of differentially expressed genes (DEGs) of each tumor subtype. (**h**)
715 Volcano plots of DEGs (upper) and gene ontology pathways (lower) differentially expressed between
716 Cushings and silent corticotroph adenomas (left) as well as between null cell adenomas and silent
717 gonadotroph adenomas (right). NCA: null cell adenoma; PRLoma: prolactinoma; SCA: silent corticotroph
718 adenoma; SGA: silent gonadotroph adenoma; CNV = copy number variant.
719
720

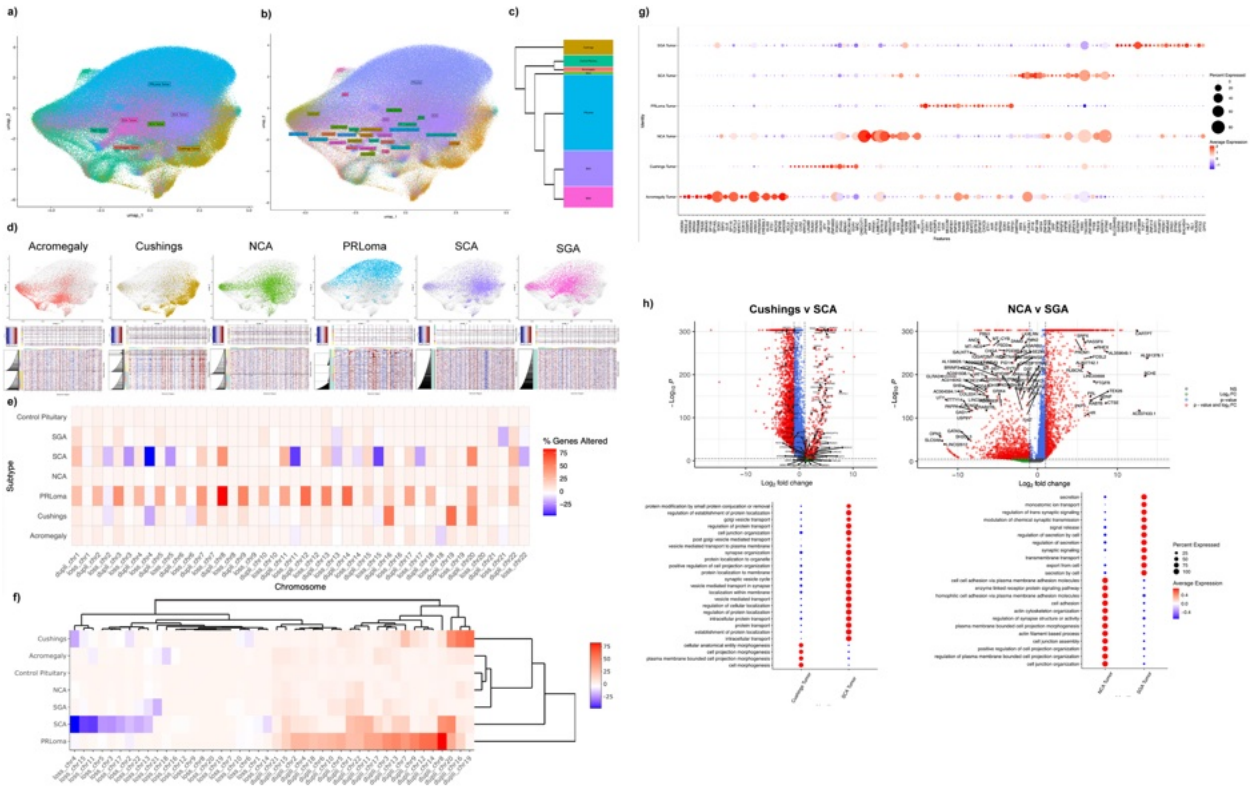
a)
b)
c)
d)
Acromegaly
Cushings
NCA
PRLoma
SCA
SGA
e)
Control Pituitary
SGA
SCA
NCA
PRLoma
Cushings
Acromegaly
Subtype
% Genes Altered
Chromosome
f)
Cushings
Acromegaly
Control Pituitary
NCA
SGA
SCA
PRLoma
g)
h)
Cushings v SCA
NCA v SGA
Log2 fold change
Percent Expressed
Average Expression

723
724
725 **Figure 3: Pseudotime trajectory analysis of pituitary neuroendocrine tumors**. (**a-e**) Dimensional
726 reduction of each tumor subtype, plotted with stem, tumor nuclei, and normal neuroendocrine counterpart
727 nuclei. For null cell adenomas, all neuroendocrine nuclei were included ("Clusters"). Similar plots re-
728 colored by pseudotime after trajectory analysis ("Trajectories"). ridge plots of demonstrating pseudotime
729 distribution of each cluster and ordered by mean pseudotime ("Pseudotime-Sorted"). Transcriptomic
730 heatmaps of RNA expression of pseudotime-correlated differentially expressed genes with either increased
731 or decreased expression in each cluster ("Pseudotime DEGs"). (**f**) post-hoc ridge plot of prolactinoma nuclei
732 after splitting prolactinomas into early and late subclusters. (**g**) pseudotime-correlated DEGs of early and
733 late prolactinoma nuclei. NCA: null cell adenoma; PRLoma: prolactinoma; SCA: silent corticotroph
734 adenoma; SGA: silent gonadotroph adenoma; DEG: differentially expressed gene.
735
736

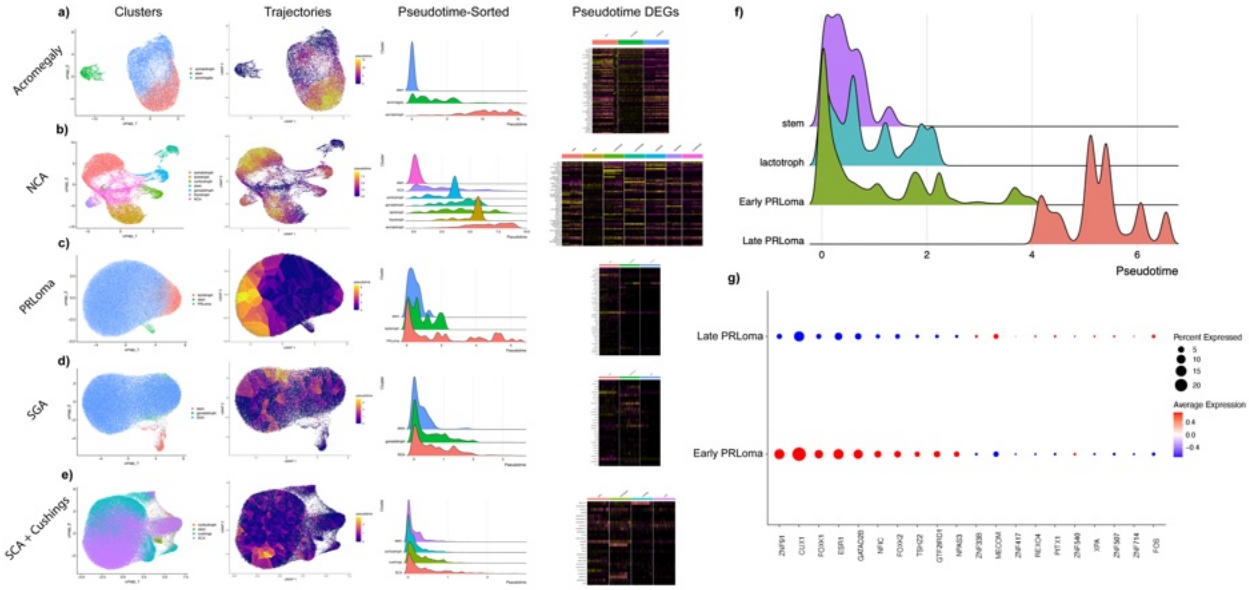
a)
Clusters
Trajectories
Pseudotime-Sorted
Pseudotime DEGs
Acromegaly
b)
NCA
c)
PRLoma
d)
SGA
e)
SCA + Cushings
f)
stem
lactotroph
Early PRLoma
Late PRLoma
0
2
4
6
Pseudotime
g)
Late PRLoma
Early PRLoma
Percent Expressed
5
10
15
20
Average Expression
0.4
0.0
-0.4
ZNF91
CUX1
FOXK1
ESR1
GATA2BB
NFIC
FOXK2
TSHZ2
GTF2IRD1
NPAS3
ZNF385
MECOM
ZNF417
RE3C4
PITX1
ZNF540
XPA
ZNF507
ZNF714
FOS

739
740 **Figure 4**: **Cell-cell communication network analysis of pituitary neuroendocrine tumors**. (**a**) overall
741 communication size and strength between nuclei types. (**b**) expression of outgoing signaling ligands of
742 nontumor nuclei in normal control samples. (**c**) expression of outgoing signaling ligands of tumor nuclei
743 and their normal neuroendocrine counterpart nuclei, clustered by expression similarity. (**d**) river plot meta-
744 clustering of normal control nuclei, where normal nuclei are sorted into "patterns" based on outgoing
745 expression of communication ligands (left). Legend demonstrating the signaling ligands associated with
746 each "pattern" (right). NCA: null cell adenoma; PRLoma: prolactinoma; SCA: silent corticotroph adenoma;
747 SGA: silent gonadotroph adenoma.
748
749

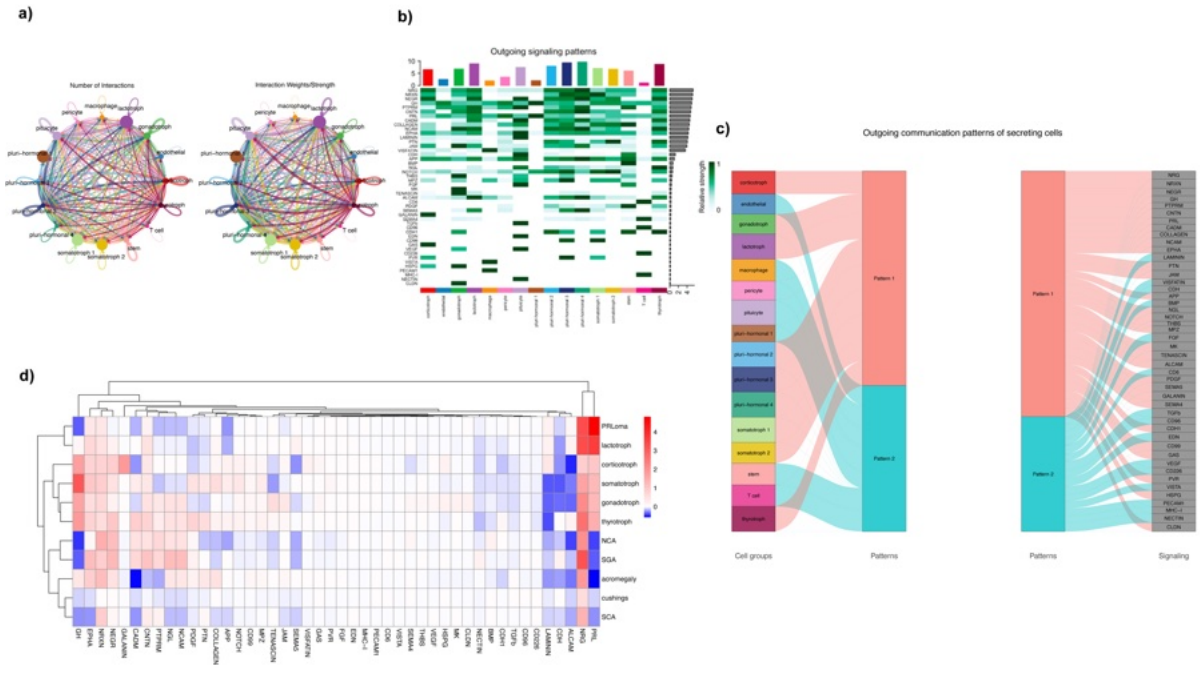
a)
Number of Interactions
Interaction Weights/Strength
b)
Outgoing signaling patterns
c)
Outgoing communication patterns of secreting cells
Relative strength
Cell groups
Patterns
Patterns
Signaling
d)
PRLoma
lactotroph
corticotroph
somatotroph
gonadotroph
thyrotroph
NCA
SGA
acromegaly
cushings
SCA

752
753 **Figure 5: Transcriptomic analysis of the pituitary microenvironment in PitNETs compared to**
754 **normal control pituitaries**. (**a**) transcriptomic expression of DEGs of stromal nuclei in PitNETs relative
755 to their counterpart nuclei in normal pituitary controls. (**b-l**) Volcano plots of all DEGs associated with each
756 stromal cell identity, plotting the expression level of each gene in tumor stroma relative to normal pituitary
757 stroma. (**m**) workflow of spatial transcriptomic analysis of tumor samples. Frozen pituitary adenomas from
758 multiple patients were embedded into a single paraffin block after thawing and fixation, then mounted on
759 a slide for GeoMx spatial transcriptomics. (**n**) Differential expression analysis comparing areas with high
760 vascularization against those with low or no vascularization highlight 15 DEGs positively enriched for in
761 vascularized areas. (**o**) An example of a tumor with four of the GeoMx ROI's, represented as white circles.
762 αSMA is stained for in red with Hoechst 33342 in teal and CD68 in green. P) The top ROI in panel C
763 representing an area of low vascularization with and without the GeoMx segmentation for tumor segments.
764 The tumor segment (grey) excludes αSMA positive pixels and CD68 positive pixels. Q) The ROI second
765 from the top in panel C, representing an area of high vascularization with and without the GeoMx
766 segmentation. The collected transcripts analyzed here are only from the tumor component, excluding the
767 αSMA segment, which is highlighted in green. DEG: differentially expressed gene; NS: not significant; FC:
768 fold-change.
769

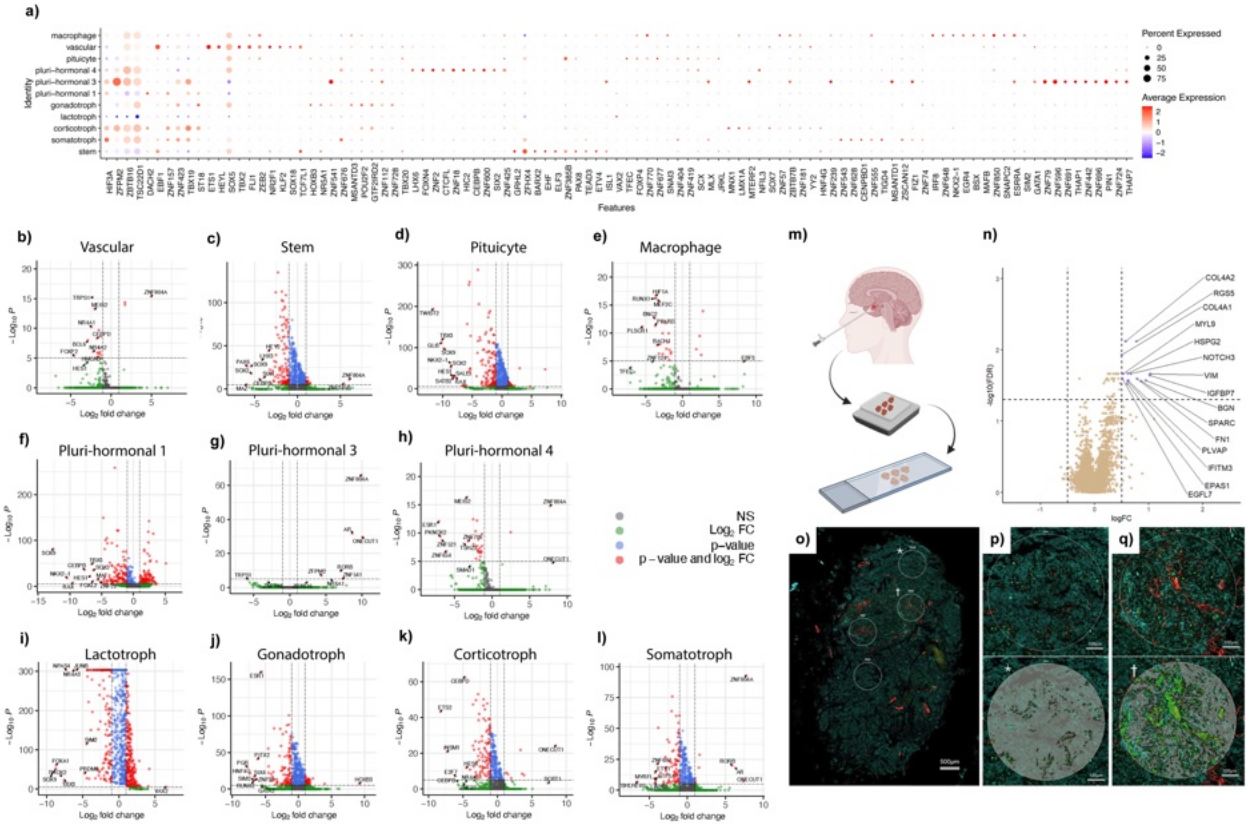
a)
Percent Expressed
Average Expression
Features
Identity
b) Vascular
c) Stem
d) Pituicyte
e) Macrophage
f) Pluri-hormonal 1
g) Pluri-hormonal 3
h) Pluri-hormonal 4
i) Lactotroph
j) Gonadotroph
k) Corticotroph
l) Somatotroph
NS
Log2 FC
p-value
p – value and log2 FC
Log2 fold change
m)
n)
COL4A2
RGS5
COL4A1
MYL9
HSPG2
NOTCH3
VIM
IGFBP7
BGN
SPARC
FN1
PLVAP
IFITM3
EPAS1
EGFL7
logFC
o)
p)
q)

772
773 **Supplementary Figure 1**: **Transcriptomic heatmaps of pseudotime-correlated differentially**
774 **expressed genes (DEGs) in normal gonadotroph cells**. DEGs expression is plotted with respect to
775 trajectory-analysis pseudotime and visualized in stem cells vs normal gonadotroph cells.
776

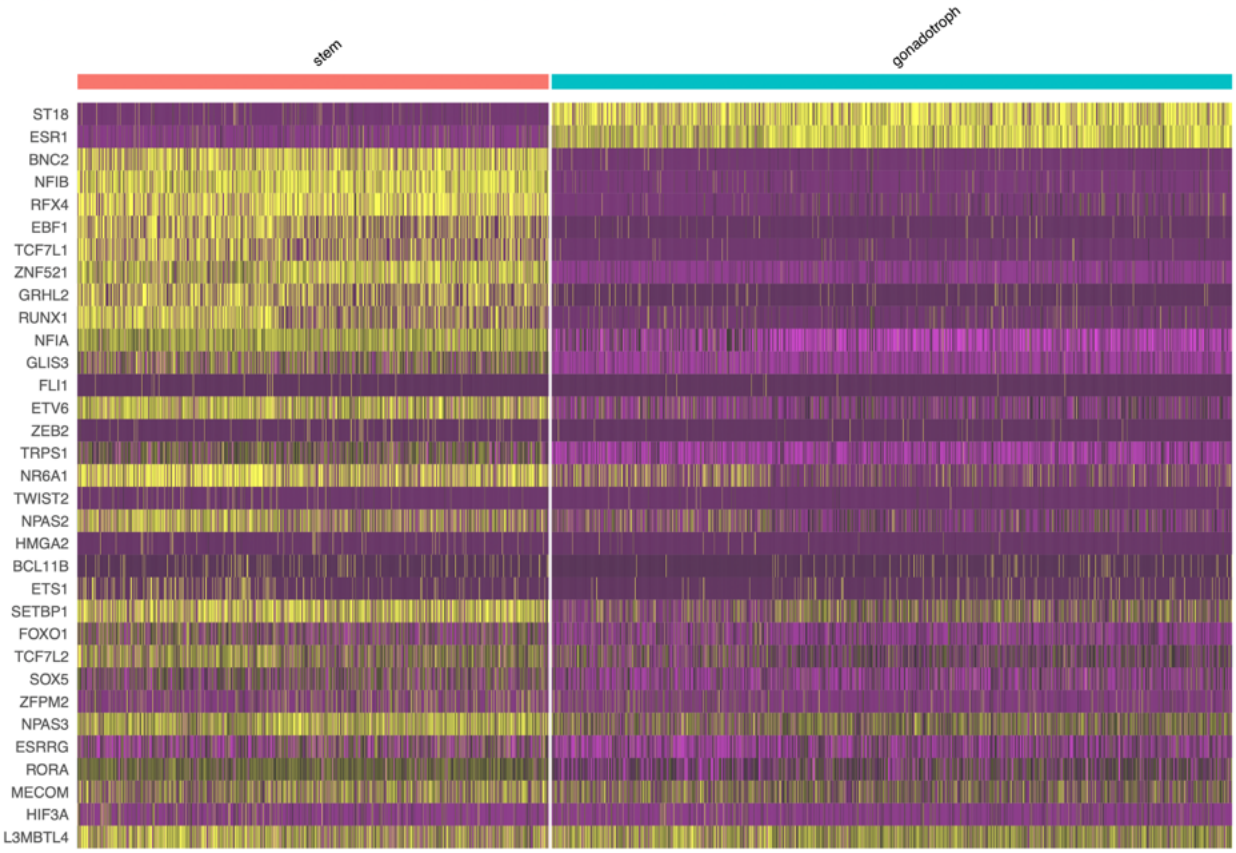
stem
gonadotroph
ST18
ESR1
BNC2
NFIB
RFX4
EBF1
TCF7L1
ZNF521
GRHL2
RUNX1
NFIA
GLIS3
FLI1
ETV6
ZEB2
TRPS1
NR6A1
TWIST2
NPAS2
HMGA2
BCL11B
ETS1
SETBP1
FOXO1
TCF7L2
SOX5
ZFPM2
NPAS3
ESRRG
RORA
MECOM
HIF3A
L3MBTL4

779
780 **Supplementary Figure 2**: **Transcriptomic heatmaps of pseudotime-correlated differentially**
781 **expressed genes (DEGs) in normal gonadotroph cells**. DEGs expression is plotted with respect to
782 trajectory-analysis pseudotime and visualized in stem cells vs cells in the "pluri-hormonal 1" cluster.
783

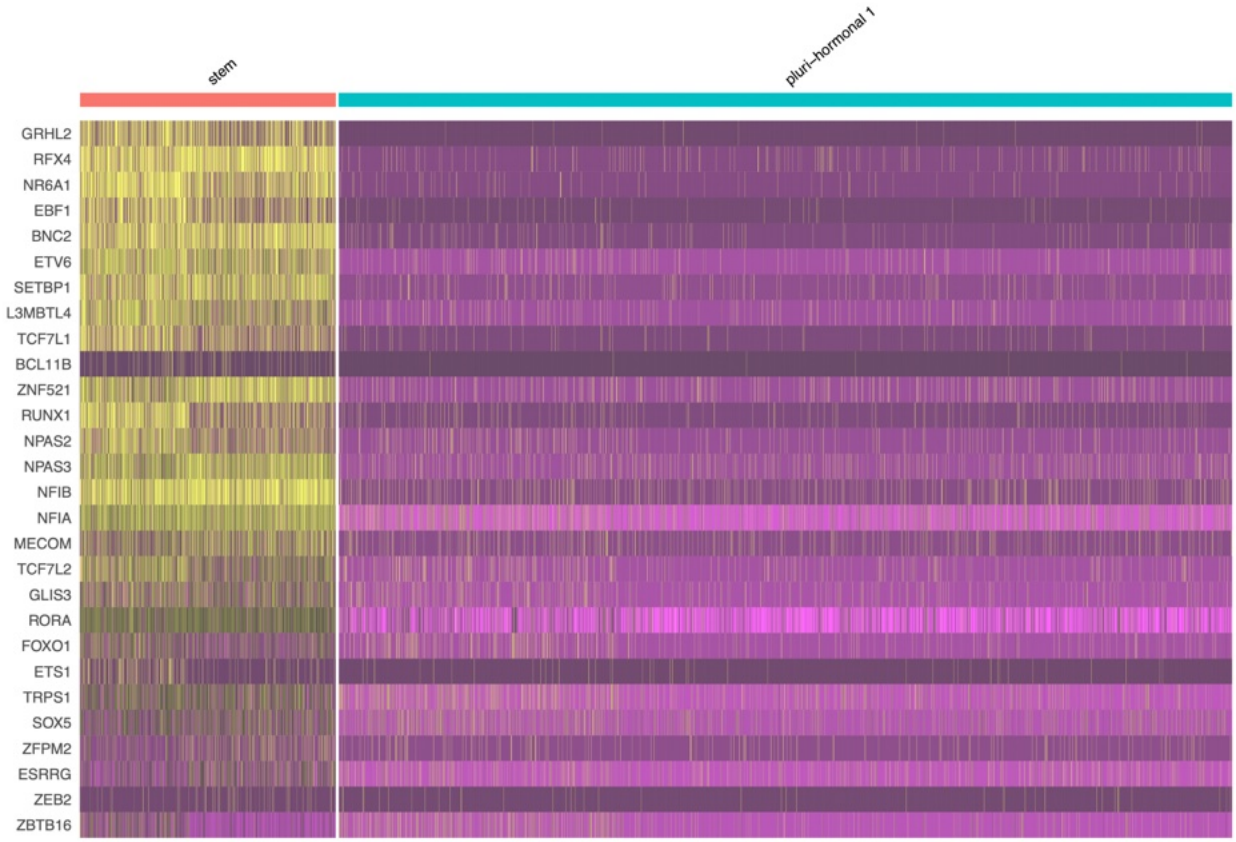
stem
pluri–hormonal 1
GRHL2
RFX4
NR6A1
EBF1
BNC2
ETV6
SETBP1
L3MBTL4
TCF7L1
BCL11B
ZNF521
RUNX1
NPAS2
NPAS3
NFIB
NFIA
MECOM
TCF7L2
GLIS3
RORA
FOXO1
ETS1
TRPS1
SOX5
ZFPM2
ESRRG
ZEB2
ZBTB16

786
787 **Supplementary Figure 3**: **Transcriptomic heatmaps of pseudotime-correlated differentially**
788 **expressed genes (DEGs) in normal gonadotroph cells**. DEGs expression is plotted with respect to
789 trajectory-analysis pseudotime and visualized in stem cells vs normal corticotroph cells.
790

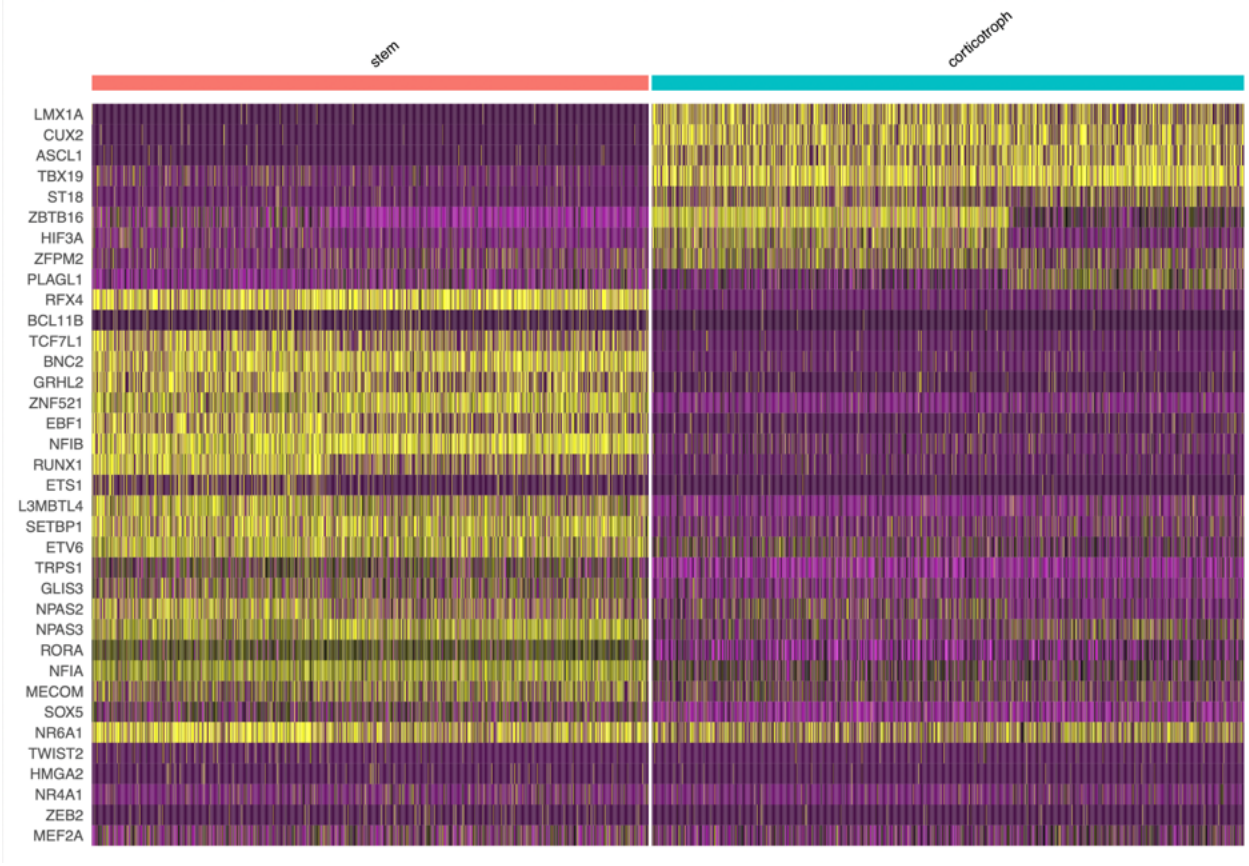
stem
corticotroph
LMX1A
CUX2
ASCL1
TBX19
ST18
ZBTB16
HIF3A
ZFPM2
PLAGL1
RFX4
BCL11B
TCF7L1
BNC2
GRHL2
ZNF521
EBF1
NFIB
RUNX1
ETS1
L3MBTL4
SETBP1
ETV6
TRPS1
GLIS3
NPAS2
NPAS3
RORA
NFIA
MECOM
SOX5
NR6A1
TWIST2
HMGA2
NR4A1
ZEB2
MEF2A

793
794 **Supplementary Figure 4**: **Transcriptomic heatmaps of pseudotime-correlated differentially**
795 **expressed genes (DEGs) in normal gonadotroph cells**. DEGs expression is plotted with respect to
796 trajectory-analysis pseudotime and visualized in stem cells vs normal lactotroph cells.
797

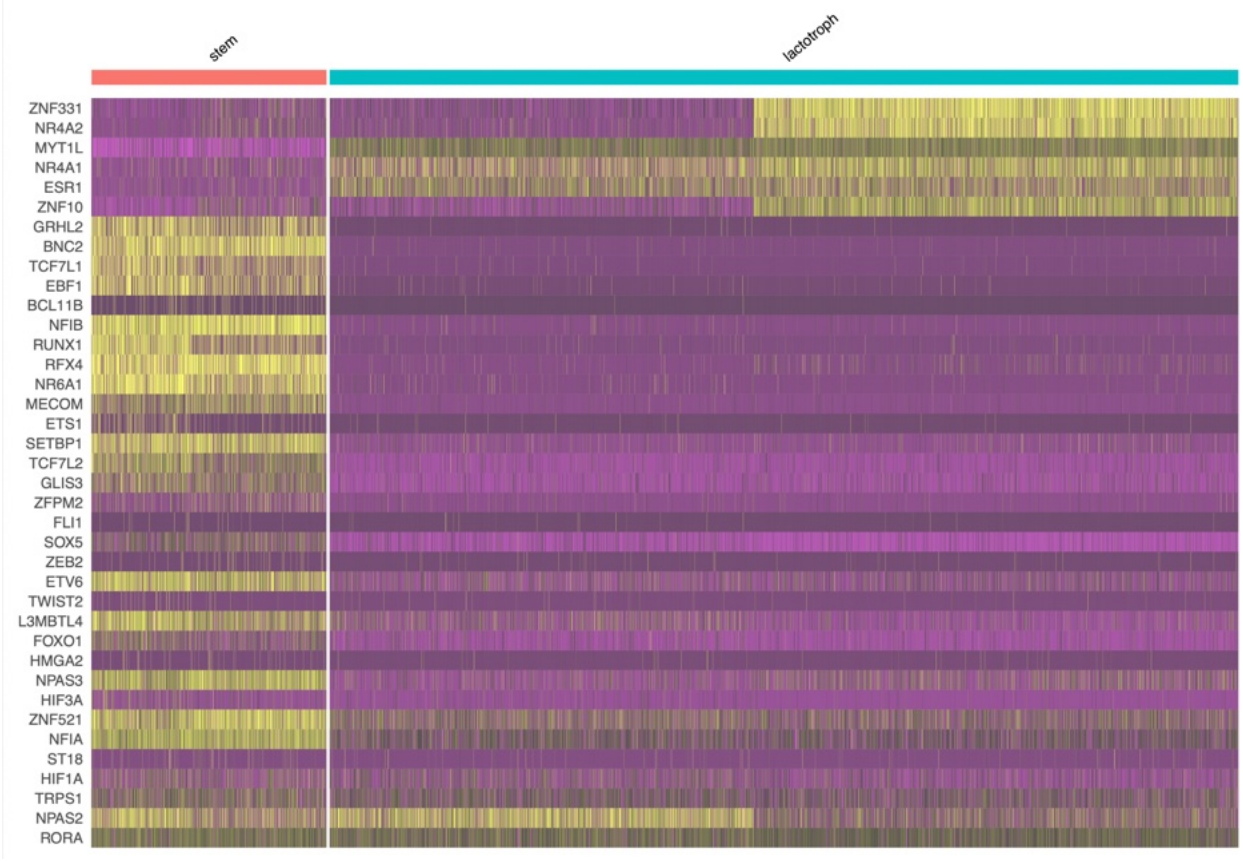
stem
lactotroph
ZNF331
NR4A2
MYT1L
NR4A1
ESR1
ZNF10
GRHL2
BNC2
TCF7L1
EBF1
BCL11B
NFIB
RUNX1
RFX4
NR6A1
MECOM
ETS1
SETBP1
TCF7L2
GLIS3
ZFPM2
FLI1
SOX5
ZEB2
ETV6
TWIST2
L3MBTL4
FOXO1
HMGA2
NPAS3
HIF3A
ZNF521
NFIA
ST18
HIF1A
TRPS1
NPAS2
RORA

800
801 **Supplementary Figure 5**: **Transcriptomic heatmaps of pseudotime-correlated differentially**
802 **expressed genes (DEGs) in normal gonadotroph cells**. DEGs expression is plotted with respect to
803 trajectory-analysis pseudotime and visualized in stem cells vs cells in the "pluri-hormonal 4" cluster.
804

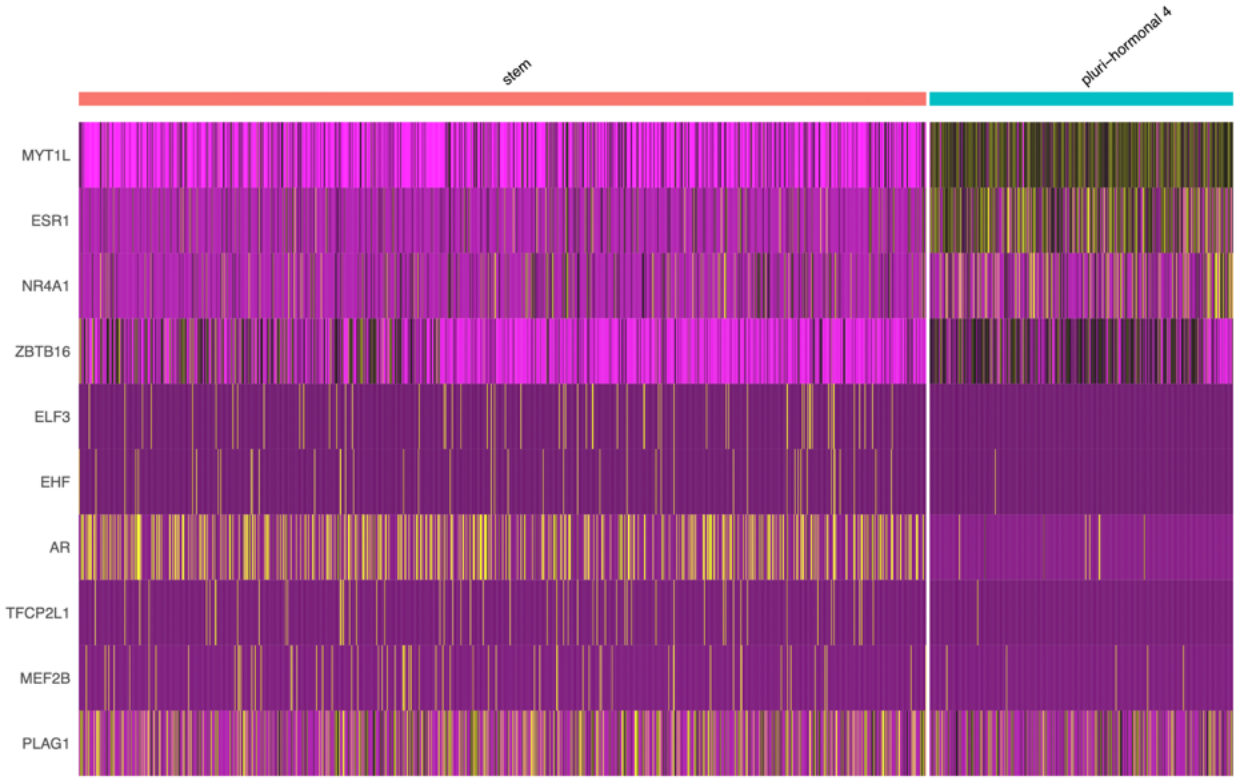
stem
pluri–hormonal 4
MYT1L
ESR1
NR4A1
ZBTB16
ELF3
EHF
AR
TFCP2L1
MEF2B
PLAG1

807
808 **Supplementary Figure 6**: **Transcriptomic heatmaps of pseudotime-correlated differentially**
809 **expressed genes (DEGs) in normal gonadotroph cells**. DEGs expression is plotted with respect to
810 trajectory-analysis pseudotime and visualized in stem cells vs cells in the "somatotroph 1" and
811 "somatotroph 2" clusters.
812

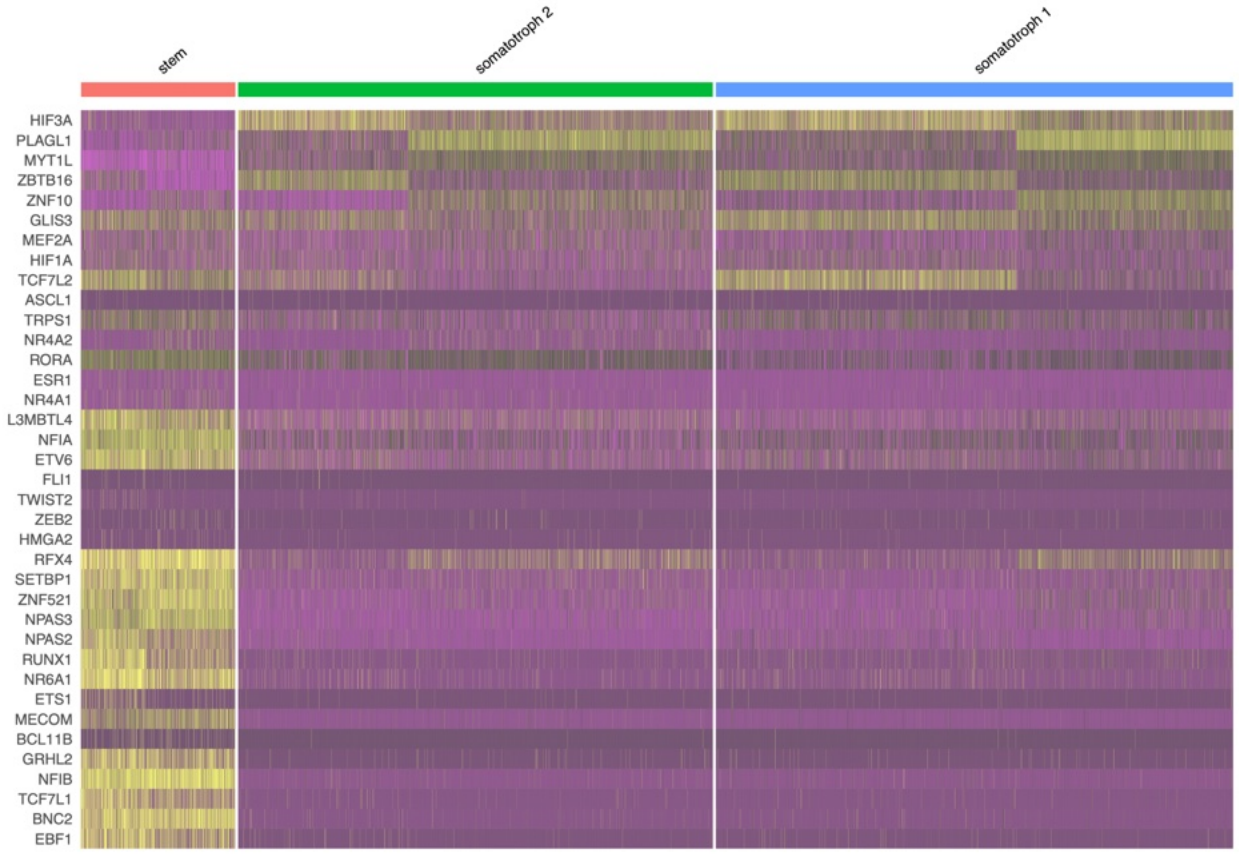
stem
somatotroph 2
somatotroph 1
HIF3A
PLAGL1
MYT1L
ZBTB16
ZNF10
GLIS3
MEF2A
HIF1A
TCF7L2
ASCL1
TRPS1
NR4A2
RORA
ESR1
NR4A1
L3MBTL4
NFIA
ETV6
FLI1
TWIST2
ZEB2
HMGA2
RFX4
SETBP1
ZNF521
NPAS3
NPAS2
RUNX1
NR6A1
ETS1
MECOM
BCL11B
GRHL2
NFIB
TCF7L1
BNC2
EBF1

815 **Supplementary Figure 7**: **Transcriptomic heatmaps of pseudotime-correlated differentially**
816 **expressed genes (DEGs) in normal gonadotroph cells**. DEGs expression is plotted with respect to
817 trajectory-analysis pseudotime and visualized in stem cells vs cells in the "pluri-hormonal 2" cluster.
818

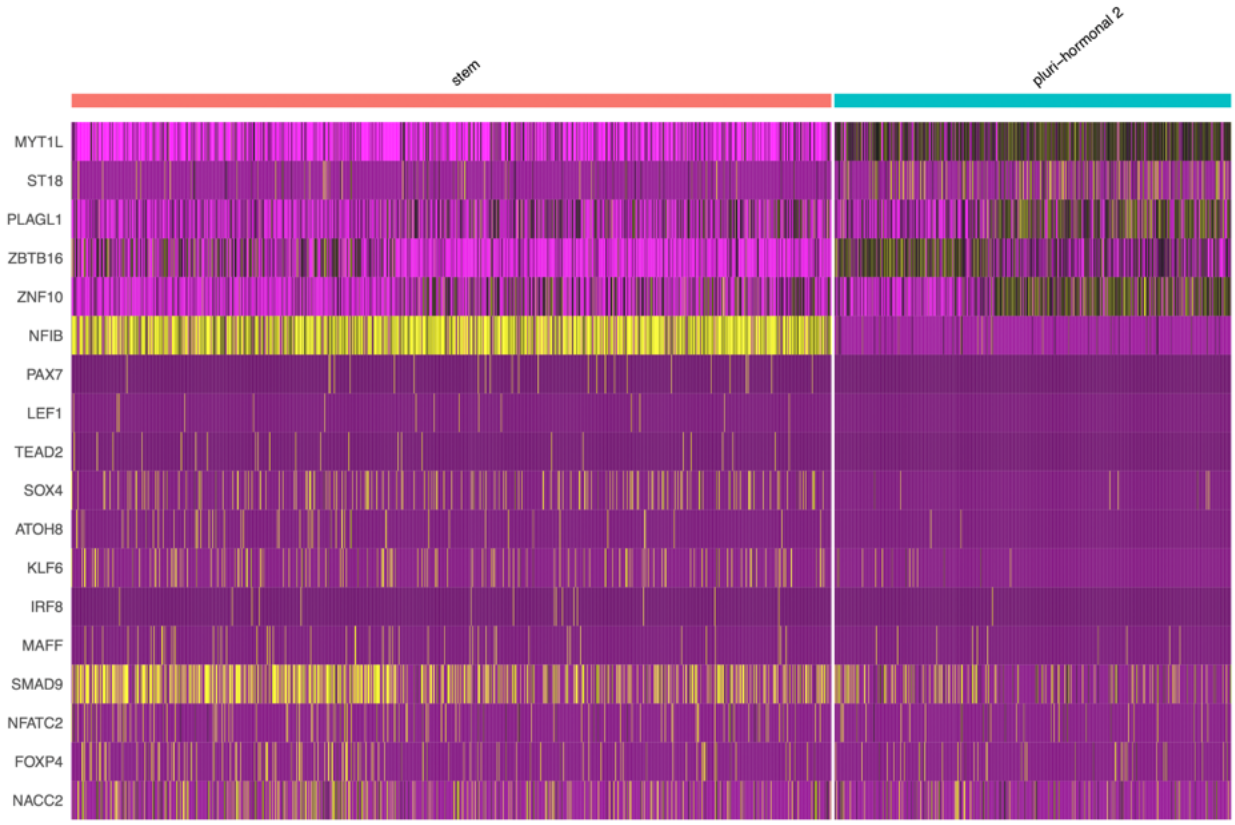
stem
pluri-hormonal 2
MYT1L
ST18
PLAGL1
ZBTB16
ZNF10
NFIB
PAX7
LEF1
TEAD2
SOX4
ATOH8
KLF6
IRF8
MAFF
SMAD9
NFATC2
FOXP4
NACC2

821
822 **Supplementary Figure 8**: **Transcriptomic heatmaps of pseudotime-correlated differentially**
823 **expressed genes (DEGs) in normal gonadotroph cells**. DEGs expression is plotted with respect to
824 trajectory-analysis pseudotime and visualized in stem cells vs thyrotroph cells.
825

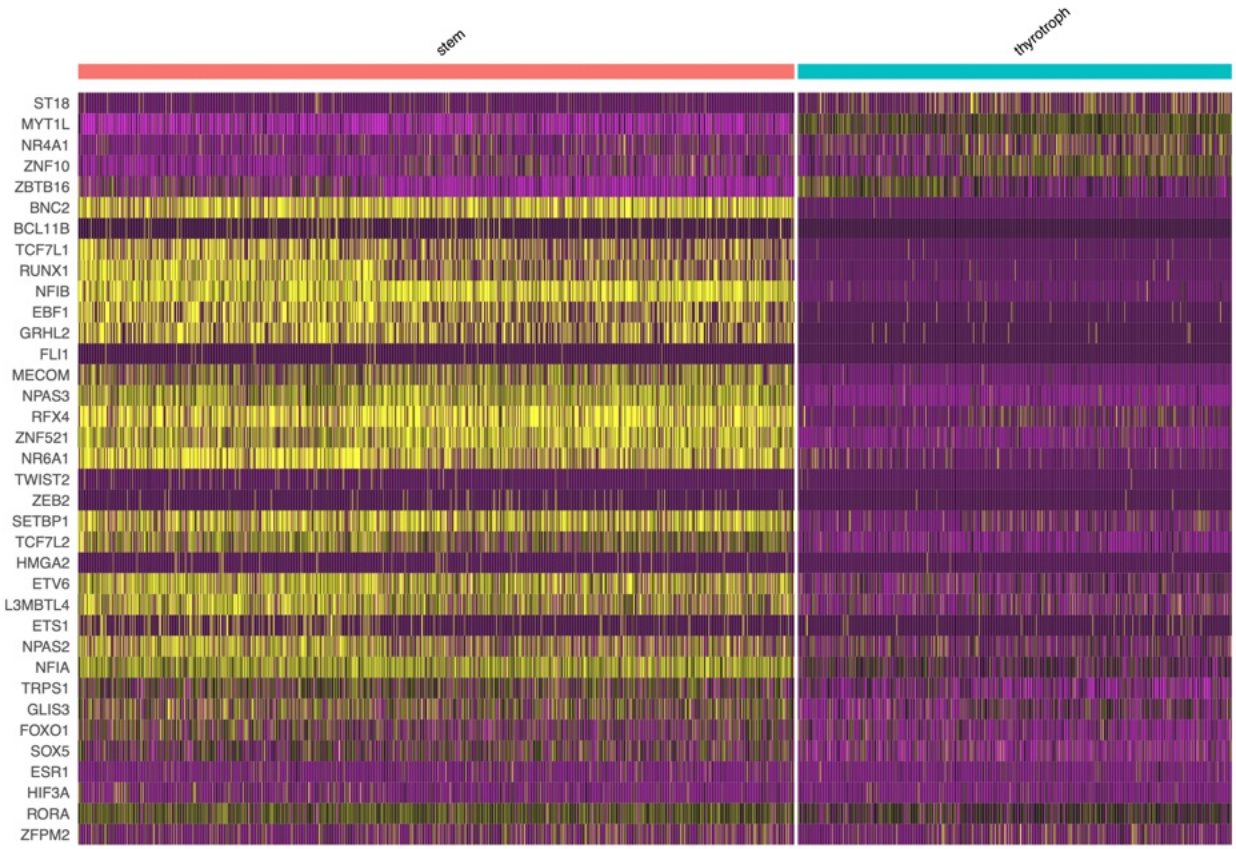
stem
thyrotroph
ST18
MYT1L
NR4A1
ZNF10
ZBTB16
BNC2
BCL11B
TCF7L1
RUNX1
NFIB
EBF1
GRHL2
FLI1
MECOM
NPAS3
RFX4
ZNF521
NR6A1
TWIST2
ZEB2
SETBP1
TCF7L2
HMGA2
ETV6
L3MBTL4
ETS1
NPAS2
NFIA
TRPS1
GLIS3
FOXO1
SOX5
ESR1
HIF3A
RORA
ZFPM2

826